Jonas Ylönen

Simulation of resonant nanostructures for electric near field enhancement

School of Electrical Engineering

Thesis submitted for examination for the degree of Master of Science in Technology.

Espoo 22.1.2018

Thesis supervisor:

Prof. Markku Sopanen

Thesis advisor:

D.Sc. Nagarajan Subramaniyam

Aalto University
School of Electrical
Engineering

Aalto University
School of Electrical Engineering

Abstract of the master's thesis

Author: Jonas Ylönen

Title: Simulation of resonant nanostructures for electric near field enhancement

Date: 22.1.2018 Language: English Number of pages:7+48

Department of Electronics and Nanoengineering

Major: Micro- and Nanosciences Code: ELEC3037

Supervisor: Prof. Markku Sopanen

Advisor: D.Sc. Nagarajan Subramaniyam

Near field enhancement is beneficial in a wide range of applications in imaging, spectroscopy and amplification of nonlinear optical processes. These often rely on using nanostructures to focus and amplify the surrounding electric field. This enhanced field is localized around the emitting feature, and requires the object it interacts with to be placed in close proximity.

This thesis investigates the structural geometry and optical phenomena of different types of resonant nanostructures designed for electric near field enhancement. The goal is to design a nanostructure that can provide a strong enhancement uniformly over its surface, making it usable as a substrate for imaging applications. The types of structures investigated are gratings, metal covered distributed Bragg reflectors (DBR) and optical cavities, which support surface plasmons, Tamm plasmons and cavity modes, respectively.

The main method of study in this thesis is finite element method (FEM) simulation. The simulations are performed in 2D geometry using transverse magnetic (TM) and transverse electric (TE) radiation. The gratings, metal covered DBR and cavities are first studied separately, then structures combining the grating and optical cavity are investigated, in an attempt to benefit from coupling between the different resonances. Finally, dielectric gratings on plain metal surfaces are examined. In addition to the simulations, some of the structures are fabricated for reflectance measurements.

The simulations managed to provide a lot of information about the resonant behaviour of the nanostructures. Structural parameters for optimal coupling of light at wavelengths close to 500 nm were discovered for many of the structures. The combinations of structures displayed evidence of coupling between the different resonant behaviours, but this coupling was not able to significantly improve the electric field enhancement. The dielectric gratings investigated at the end proved more promising for imaging applications.

Keywords: near field enhancement, surface plasmon, Tamm plasmon, optical cavity, finite element method, simulation

Aalto-yliopisto
Sähkötekniikan korkeakoulu

Diplomityön tiivistelmä

Tekijä: Jonas Ylönen

Työn nimi: Sähköisen lähikentän vahvistamiseksi suunniteltujen resonanttien nanorakenteiden simulointi

Päivämäärä: 22.1.2018 Kieli: Englanti Sivujen lukumäärä:7+48

Elektroniikan ja nanotekniikan laitos

Pääaine: Mikro- ja nanotekniikka Koodi: ELEC3037

Valvoja: Prof. Markku Sopanen

Ohjaaja: D.Sc. Nagarajan Subramaniyam

Lähikentän vahvistamista hyödynnetään monissa kuvantamiseen, spektroskopiaan ja epälineaarisien prosessien tehostamiseen liittyvissä sovelluksissa. Nämä hyödyntävät usein nanorakenteita jotka keskittävät ja vahvistavat ympäröivää sähkökenttää. Vahvistettu kenttä keskittyy yleensä rakenteiden ympärille, ja vaatii tämän kanssa vuorovaikutuksessa olevan objektin sijoittamisen niiden lähelle.

Tämä diplomityö tutkii erilaisten sähköisen lähikentän vahvistamiseen suunniteltujen resonoivien nanorakenteiden rakenteellisia mittoja sekä niissä tapahtuvia optisia ilmiöitä. Tavoitteena on suunnitella nanorakenne joka kykenee tehokkaasti vahvistamaan sähkökenttää tasaisesti pintansa yllä, jota voitaisiin soveltaa näytealustana kuvantamisessa. Tutkittavia rakenteita ovat hilat, metallipäällysteiset Bragg-heijastimet (DBR) sekä optiset kaviteetit, jotka tukevat pintaplasmoneja, Tamm-plasmoneja sekä kaviteettimoodeja.

Tämän diplomityön pääasiallinen tutkimusmenetelmä on yleiseen elementtimenetelmään (FEM) perustuva simulointi. Simuloinnit suoritetaan 2D-geometriassa, käyttäen poikittaisen magneettikentän (TM) ja poikittaisen sähkökentän (TE) mukaisesti polarisoitua säteilyä. Hilaa, metallipäällysteistä DBR:ää sekä kaviteettia tutkitaan ensin erikseen, jonka jälkeen tutkitaan rakenteita, joissa yhdistyvät hila ja kaviteetti, tarkoituksena hyötyä näiden rakenteiden eri resonanssien välisestä kytkeytymisestä. Lopuksi tutkitaan sileiden metallipintojen päälle sijoitettuja dielektrisestä aineesta valmistettuja hiloja. Simulaatioiden lisäksi jotkin rakenteista valmistetaan heijastussuhteen mittaamiseksi.

Simulaatiot onnistuivat tuottamaan paljon tietoa nanorakenteiden resonoivasta käyttäytymisestä. Monille rakenteista löytyivät optimaaliset rakenteelliset parametrit kytkeytymiseksi valoon 500 nm:n aallonpituudella. Yhdistetyt rakenteet osoittivat merkkejä erillisten resonanttien käytösten välisestä kytkeytymisestä, mutta tämä ei tarjonnut huomattavaa parannusta sähkökentän vahvistukseen. Lopuksi tutkitut dielektriset hilat osoittautuivat lupaavammiksi kuvantamistarkoitukseen.

Avainsanat: lähikentän vahvistus, pintaplasmoni, Tamm plasmoni, optinen kaviteetti, yleinen elementtimenetelmä, simulointi

Preface

The work presented in this thesis was carried out at the Department of Electronics and Nanoengineering at Aalto University School of Electrical Engineering. I wish to offer my thanks to my supervisor Markku Sopanen and my advisor Nagarajan Subramaniyam for giving me the opportunity to work on my Master's thesis in connection to an interesting project, and for their assistance with the thesis. I also wish to aknowledge Nagarajan for manufacturing the samples used in the measurements. I also wish to express my gratitude to Hanne Ludvigsen for helping me to stay informed of the practicalities connected to the Master's thesis. Finally, I wish to thank my parents Pertti Ylönen and Birgitta Klärich-Ylönen for their support throughout my studies.

Espoo, 22.1.2018

Jonas Ylönen

Contents

Symbols and abbreviations

Symbols

A_{port1}	Area of port 1
c	Speed of light in vacuum
d	Thickness of layer
E	Electric field
E_0	Input electric field
I	Electric field intensity
I_0	Input electric field intensity
k	Wave vector
k_0	Free space wave vector
ñ	Complex refractive index
n	Real refractive index
P_{in}	Input power
R	Reflectance
T	Transmittance
ε	Permittivity
ε_0	Vacuum permittivity
ε_r	Relative permittivity
ε'_r	Real part of relative permittivity
ε''_r	Complex part of relative permittivity
κ	Extinction coefficient
λ	Wavelength
λ_0	Vacuum wavelength
μ_r	Relative permeability
σ	Conductivity
φ	Phase shift

ω	Angular frequency

Abbreviations

Ag	Silver
ALD	Atomic layer deposition
Au	Gold
DBR	Distributed Bragg reflector
FEM	Finite element method
SERS	Surface enhanced Raman sacattering
SPR	Surface plasmon resonance
SNOM	Near field scanning optical microscopy
Si	Silicon
TE	Transverse electric
TM	Transverse magnetic

1 Introduction

The electromagnetic near field region extends from the surface of an object to a distance of roughly one wavelength, which for visible light is on the scale of a few hundred nanometer. The near field largely consists of non-radiative field components, which do not carry energy into the far field region. This allows very high field intensities to form in the near field region, under certain conditions. Despite not being able to transmit energy over large distances, these fields can couple to objects placed within the near field region, allowing transfer of energy. Many measurement and imaging technologies are able to take advantage of this, such as surface enhanced Raman spectroscopy (SERS) [1], surface plasmon resonance (SPR) sensors [2, 3] and near field scanning optical microscopy (SNOM) [4].

This thesis will investigate the electric near field enhancement created by different resonant structures. These structures are all able to capture the light incident upon them, matching their resonant wavelength, and confine it into a resonant mode in the structure. This can cause very strong electric fields to form at some points in the near field region, which can enhance the response of nearby objects. One potential use is enhancement of fluorescent particles. Fluorescent particles are markers used in bio imaging, highlighting features in cells and other imaged objects [5]. These particles are usually excited at one wavelength of light, and emit light at another wavelength. They often absorb light very inefficiently, causing a high light intensity or a large number of fluorescent particles being required. By increasing the intensity of the electric field around these particles, the absorption can be enhanced, allowing improved images with less intensity. It has been shown that placing the sample a suitable distance from a reflective surface can enhance the absorption, due to a standing wave being created in the near field upon reflection [6]. The standing wave causes the intensity of the electric field to oscillate near the reflective surface, with up to a four times stronger field at the peaks of the wave. It is also possible to enhance the fluorescence of these particles by placing them near metallic nanoparticles [7], however these are only able to provide enhancement a short range from the nanoparticle. By applying nanostructures to a reflective surface, it is possible to provide a high enhancement of the electric field over a larger area, potentially enabling a very efficient enhancement of the absorption in fluorescent particles.

The structures investigated in this thesis will consist of periodic metallic gratings used to excite surface plasmons, optical cavities exhibiting cavity resonances and metal covered distributed Bragg reflector (DBR) structures used to excite Tamm plasmons. The main focus will be on exciting a strong electric field on top of the structured surface, so that these structures can be used as substrates for imaging. This is best achieved by surface plasmons, a type of surface wave occurring at the interface between a conductive metal and a dielectric. Because this wave is confined to a small distance from the surface, the electric field can achieve high intensities. Surface plasmons have been studied for applications involving imaging and sensing, as well as electronics [8, 9]. However, surface plasmons are only able to couple to waves polarized perpendicular to the grating, causing some losses in coupling efficiency for unpolarised light. The Tamm plasmon is a recently suggested structure, which could remedy this. A Tamm plasmon is formed at the interface between a DBR and a reflective metal layer, and is able to couple to both polarizations.

Another type of resonant structure is the optical cavity, which can couple to both transverse electric (TE) and transverse magnetic (TM) polarized light. The electric field enhancement in the cavity is confined inside the cavity however, unable to reach the

surface of the structure. By combining the cavity with a grating, it could be possible to extract this field.

2 Background

This thesis aims to study the electric field enhancement achievable in different resonant nanostructures. The main interest is in achieving a high electric field at the boundary between air and the investigated structure. To this end, three types of structures will be investigated. These are metallic gratings supporting surface plasmons, Tamm plasmonic structures consisting of a DBR covered by a metal layer, and optical cavities consisting of two metallic mirrors with a thin dielectric spacer between them. Surface plasmons are able to create strong electric fields at the boundary between air and a metal surface, decaying exponentially with distance from the surface. However, surface plasmons can only be excited by light polarized perpendicular to the grating, causing some loss in the coupling efficiency. Cavities are resonant structures which can confine light inside them, enhancing the electric field in the cavity. Cavities work with all polarizations of light, but provide no enhancement outside the cavity. Tamm plasmons are a proposed resonant mode, created in a DBR covered by a layer of reflective metal. Tamm plasmons are also able couple to all polarizations of light. In this section, the theoretical background of each of these phenomena will be presented, while later sections will focus on simulations and measurements of the related structures.

2.1 Surface plasmon

Surface plasmons, or surface plasmon polaritons, play a key role in many applications focused on enhancing the electric near field. These rely on either exciting localized surface plasmons around metallic nanoparticles [10], or propagating surface plasmons on continuous metal surfaces [11]. In both cases, the surface plasmons can provide a greatly enhanced electric field close to the metal.

A surface plasmon is a surface wave propagating along the boundary between a metal and a dielectric material. It consists of coherent oscillations of the conduction band electrons at the surface of the metal, coupled with an electromagnetic field. The motion of the electrons near the interface excites the electromagnetic field, extending a short distance into both the metal and dielectric materials. This field dissipates with distance from the surface, making it unable to propagate in a direction away from the boundary in either material, causing a wave localized at the metal surface. This is referred to as a surface plasmon polariton, as it contains both electron oscillations (plasmon) and electromagnetic field components (polariton). The electromagnetic field is contained at the metal surface by the high reflectance of the metal and the evanescent nature of the field in the dielectric medium. This creates a surface wave only able to propagate in a direction parallel to the surface. [12, 13]

Surface plasmons are usually characterized by their dispersion relation. In free space, light propagates with the wave vector

$$k_0 = \frac{2\pi}{\lambda} = \frac{\omega}{c}, \tag{1}$$

where λ is the vacuum wavelength, ω stands for the angular frequency and c is the speed of light in vacuum. A surface wave propagating along a horizontal x-direction has a complex wave vector $k = k_x + ik_y$, where k_x is the component parallel to the surface and k_y the component normal to it. An imaginary k_y means that the wave in this direction is evanescent, *i.e.*, it will decay within the near field and cannot transmit energy through

the far field. This wave will be strongest at the metal surface, and decay away from it. For the wave component parallel to the surface applies

$$k_x = \frac{\omega}{c}\sqrt{\frac{\varepsilon_1\varepsilon_2}{\varepsilon_1+\varepsilon_2}}, \tag{2}$$

where ε_1 is the relative permittivity of the metal and ε_2 is the relative permittivity of the dielectric. According to the boundary conditions governing electromagnetic waves, this component must be equal in both materials. At a metal-air interface this simplifies to

$$k_x = \frac{\omega}{c}\sqrt{\frac{\varepsilon_1}{\varepsilon_1+1}}. \tag{3}$$

The wave vector components normal to the surface satisfy the equations

$$k_{y1} = \frac{\omega}{c}\frac{\varepsilon_1}{\sqrt{\varepsilon_1+\varepsilon_2}} \tag{4}$$

for the wave in metal, and

$$k_{y2} = \frac{\omega}{c}\frac{\varepsilon_2}{\sqrt{\varepsilon_1+\varepsilon_2}} \tag{5}$$

for the wave in dielectric. For a metal-air boundary these simplify to

$$k_{y1} = \frac{\omega}{c}\frac{\varepsilon_1}{\sqrt{\varepsilon_1+1}} \tag{6}$$

and

$$k_{y2} = \frac{\omega}{c}\frac{1}{\sqrt{\varepsilon_1+1}}. \tag{7}$$

Both k_{y1} and k_{y2} become imaginary when $\varepsilon_1 < -\varepsilon_2$, *i.e.*, when the relative permittivity of the metal is strongly negative. This is a necessary condition for the existence of a surface plasmon. Additionally, for a realistic solution to exist, the metal also needs to be slightly lossy, expressed as a small imaginary component of its relative permittivity. This causes k_x to have a small imaginary component, indicating a slight loss in the surface plasmon propagation, and k_{y1} and k_{y2} to have small real components. The above conditions cause the square root in equation 2 to become larger than one, causing k_x to be larger than k_0. This causes the phase velocity $\frac{\omega}{k}$ of the surface plasmon to be smaller than that of light propagating freely in the dielectric, making the wavelength of the surface plasmon shorter than that of freely propagating light. Due to this, surface plasmons cannot be directly excited by incident light, or radiate light themselves, allowing them to stay bound to the surface. Because of this, special means are needed to couple light to surface plasmon.

The most common ways to overcome the mismatch in phase velocity are coupling using either a prism or a metal grating. Prism coupling can be arranged either in Kretchmann-Raether configuration [14], in which a thin metal film is deposited on the surface of a prism, or Otto configuration [15], in which a prism is placed a short distance above a metal surface. In both cases coupling to the surface plasmons is facilitated by evanescent waves. These are generated through total internal reflection of light incident

on the interface between the prism and air at an angle above the critical angle. The addition of the metal surface causes frustrated total internal reflection, where the evanescent wave is able to transfer energy to the metal, allowing a surface plasmon to form. In Kretchmann-Raether configuration the evanescent wave is excited on the metal-air interface opposite from the prism, allowing a surface plasmon to form. In Otto configuration the evanescent wave is excited at the prism-air interface and a metal surface is placed within the decay distance of the evanescent wave, allowing it to couple to the metal surface. The evanescent wave matches the exponentially decaying field component of the surface plasmon, normal to the surface, allowing coupling with the surface wave. This surface plasmon is then able to propagate a distance along the surface, limited by the attenuation in the metal. The simplest way to experimentally observe the excitation of surface plasmons in either prism coupling scheme is by measuring the angular reflectance at a certain wavelength. The coupling to the surface plasmon will be noticeable as a dip in the angular reflection spectrum at an angle slightly higher than the angle for total internal reflection. Because the surface plasmon has electric field components both along the surface and normal to it, prism coupling requires TM polarized light to excite surface plasmons, *i.e.*, light with the electric field components lying in the plane of incidence [15]. Figure 1 demonstrates the angular reflectance spectrum in a simultion of the Kretchmann-Raether configuration, with light incident on a 50 nm thick layer of gold through a glass prism. Figure 1 also shows the electric field component normal to the surface at the resonant angle.

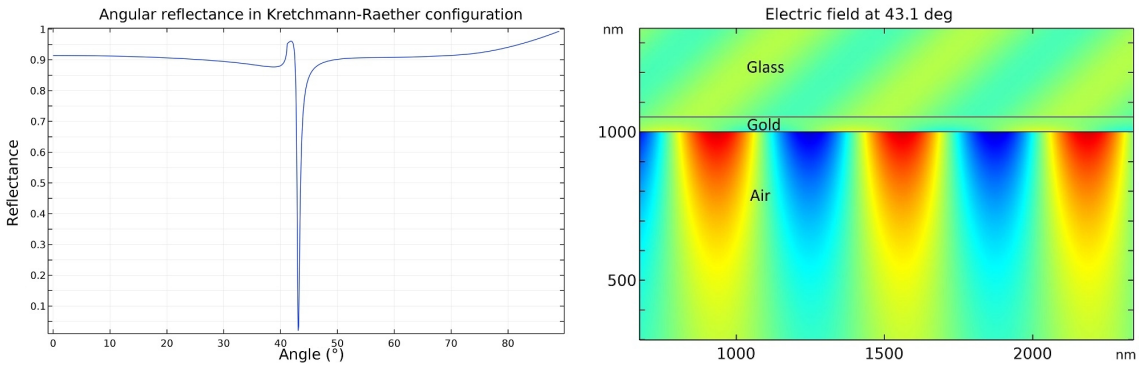

Figure 1: Angular reflectance and electric field perpendicular to surface in prism coupling using Kretchmann-Raether configuration. The resonant wavelength is visible as a sharp dip in the reflectance, at an angle slightly above the critical angle. This excites a surface wave at the gold-air interface. The red and blue colours symbolize a positive and negative electric field respectively.

In grating coupling, surface plasmons are excited by light incident on a grating located on the surface of the metal. The metal grating causes the light to scatter, allowing it to overcome the phase velocity mismatch [16]. In fact, even some roughness on an otherwise smooth metal surface can cause sufficient scattering to excite surface plasmons [17]. When excited by incident light, metal gratings are able to generate two types of surface plasmons, localized surface plasmons [18] and propagating surface plasmons [19]. The localized surface plasmons can cause very high enhancements of the electric field around the grating edges, but this enhancement is confined to a range of only a few nanometers. Propagating surface plasmons provide a lesser enhancement of the electric field at the surface, but this electric field is able to extend further and can provide a notable enhancement several hundreds of nanometers from the surface. The propagating

surface plasmons enhance the electric field on top of the grating, near the grating edges, and are able to propagate some distance similarly to the surface plasmons excited through prism coupling. In this thesis, only the propagating surface plasmons will be examined, due to their ability to provide electric field enhancement more uniformly over the grating surface, and extend this enhancement to a significant distance. Excitation of surface plasmons through grating coupling can be observed as a sharp dip in the reflectance spectrum of light incident on the grating. The wavelength of this dip depends on the dimensions of the grating and the angle of incidence. Grating coupling also requires the incident light to be TM polarized, *i.e.*, its electric field being perpendicular to the grating.

As shown previously, surface plasmons require a metal with a strongly negative real component of dielectric constant, and a small nonzero imaginary component. The optical behaviour of materials is commonly expressed through their complex refractive indices

$$\tilde{n} = (n - i\kappa), \tag{8}$$

where n stands for the real component of the refractive index, indicating the phase velocity of a plane wave in the material, and k stands for the extinction coefficient, indicating attenuation in the material. The refractive index is related to the relative permittivity through

$$\tilde{n} = \sqrt{\varepsilon_r \mu_r}, \tag{9}$$

where ε_r is the complex relative electric permittivity and μ_r is the relative magnetic permeability. The materials used in this thesis can be approximated as nonmagnetic in the examined optical wavelength range. This simplifies the above equation to

$$\tilde{n} = \sqrt{\varepsilon_r}, \tag{10}$$

which expands to

$$(n - ik) = \sqrt{\varepsilon'_r - i\varepsilon''_r}. \tag{11}$$

Here ε'_r is the real part of the relative permittivity and ε''_r the complex part. From equation 11, the real part becomes

$$\varepsilon'_r = n^2 - \kappa^2 \tag{12}$$

and the imaginary

$$\varepsilon''_r = 2n\kappa. \tag{13}$$

Based on these equations, the requirements for the metal to support surface plasmons can be expressed in terms of refractive index. For ε'_r to be strongly negative, κ needs to be larger than n, while a small ε''_r requires $n\kappa$ to be small and both n and κ to be nonzero. This leads to conditions that n should be very small, while κ needs to be significantly larger than n.

These requirements are best fulfilled in the optical range by noble and alkaline metals, although the noble metals are commonly preferred due to their stability and ease of fabrication [20]. Especially gold (Au) and silver (Ag) are commonly used in plasmonic applications. Gold is preferred in some sensing applications due to its biocompatibility and chemical stability, while silver exhibits the lowest losses in the visible range and the ability to propagate surface plasmons furthest [21]. In this thesis both gold and silver will be investigated. Gold is the preferred material because it is highly resistant to oxidation

and it is easier to fabricate smooth surfaces from it. However gold cannot be used in plasmonic applications at wavelengths below 500 nm, because of interband transitions occurring below this wavelength, causing an increased absorption. This can be seen in the reflectance spectrum shown in figure 2, where the reflectance of gold drops sharply between 550 nm and 500 nm. This is also visible in the $n - \kappa$ spectrum gold, where k is much higher than n at wavelengths above 500 nm, but the two lie very close to each other at wavelengths below 500 nm. For silver, this behaviour occurs at 350 nm, allowing it to remain highly reflective at wavelengths above. At wavelengths lower than this aluminium could be used as plasmonic material, but it is less effective than gold or silver [21].

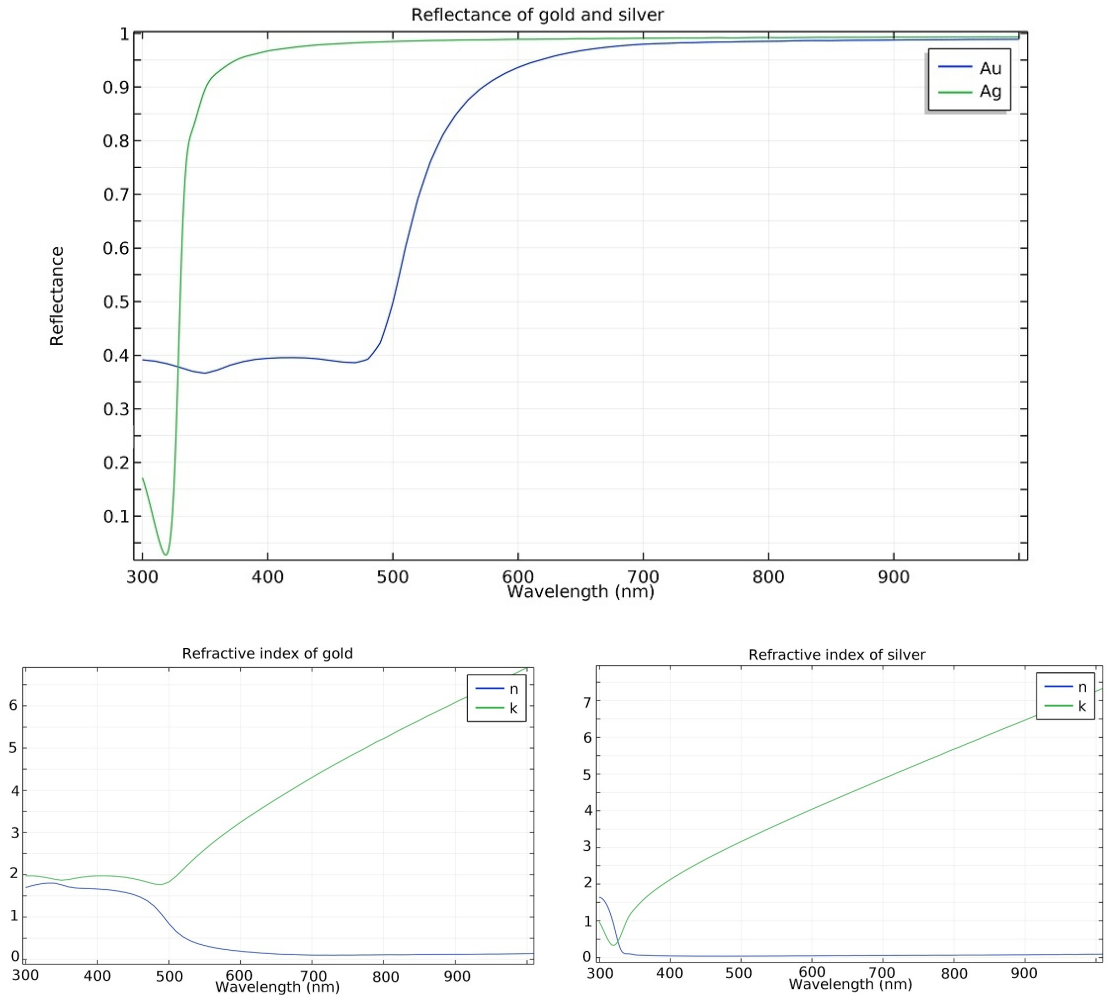

Figure 2: Reflectance spectra of both gold and silver on top, and the $n - \kappa$ spectra of gold and silver respectively below. These spectra show how the reflectance of gold starts to decrease at 550 nm and that of silver at 350 nm.

2.2 Tamm plasmon

A Tamm plasmon is a confined mode of light, formed at the interface between a DBR and a metal layer [22]. Because the DBR is an integral part of the Tamm plasmon structure, it is necessary to examine both the DBR itself and a DBR covered by a metal layer.

A DBR, or a dielectric mirror, is a multi-layered dielectric structure, which exhibits a very high reflectance at a certain range of wavelengths. This wavelength range is commonly referred to as an optical stopband, due to the transmission of light through the structure, within the wavelength range, being prevented. A DBR is created by stacking alternating layers of a high and low refractive index material on top of each other. This causes a reflection to occur at each of the interfaces between the two materials, which at normal incidence equals to

$$R = \left|\frac{n_1 - n_2}{n_1 + n_2}\right|^2 . \tag{14}$$

Here R is the reflectance of a single boundary between two materials, while n_1 and n_2 are the refractive indices of the two materials. The effects of these multiple reflections add on each other, causing a high overall reflectance. The thicknesses of the material layers are also chosen in such a way, that the reflection from each boundary interferes constructively with the reflection from the previous similar boundary, for light reflected towards the incident side. Reflections towards the transmitting side, on the other hand, experiences destructive interference. This is possible because light reflected from a low to high refractive index boundary receives a phase shift equal to π, while light reflected from a high to low refractive index boundary receives no phase shift. Due to the effects of the interference, maximal reflectivity will occur at wavelengths matching two times the thickness of two layers, *i.e.*,

$$\lambda_0 = \frac{2}{m}(n_1 d_1 + n_2 d_2), \tag{15}$$

where λ_0 is the wavelength of maximal reflectance, m is any positive integer and d_1 and d_2 are the thicknesses of the high and low refractive index material. The reflective band is centred on this wavelength, with the peak becoming flatter as the amount of layer increases. Normally the materials are stacked in an odd number of layers, with the high refractive index material being both the first and last layer of the structure. This causes the reflectance at the central wavelength to be equal to [23]

$$R = \frac{1 - \frac{n_1}{n_2}^{\frac{N-1}{2}} \frac{n_1^2}{n_a n_b}}{1 + \frac{n_1}{n_2}^{\frac{N-1}{2}} \frac{n_1^2}{n_a n_b}}^2 , \tag{16}$$

where N is the total number of layers and n_a and n_b are the refractive indices of the materials on both sides of the DBR. Usually both the individual material layers of the DBR are chosen to have an optical thickness off a quarter wavelength, as this provides the optimal reflectance [23]. The angular reflectance of a DBR is highly dependent of the polarization of the incident wave. The reflectance of TE polarized light increases with increasing angle, while TM polarized light experiences lowered reflectance with increasing angle. Both polarizations also experience a lowering of the reflective wavelength with increasing angle.

The Tamm plasmon is a resonant optical mode formed when a highly reflective layer of metal is added on top of the DBR. The high reflectance of the metal layer and DBR create a confined mode between the metal and DBR, allowing incident light to couple in to the structure. This causes a strong electric field to form inside the DBR, with an intensity peak close to the metal boundary [22]. For a Tamm plasmon to form, the metal needs to be highly reflective at the desired wavelength range and the DBR needs to

have a stopband in that same range. At optical wavelengths, the same requirements apply for the metal, as were discussed previously in relation to surface plasmons. The dielectric materials need to be transparent at the desired wavelengths, and have a sufficiently large difference in refractive indices. A Tamm plasmon can be observed as a narrow dip in the reflectance spectrum, at the resonant wavelength of the structure. This can also result in a peak in the transmission spectrum, at the same wavelength, depending on how well the electric field is contained in the structure. The resonant wavelength of the structure is usually at a wavelength slightly higher than the centre wavelength of the DBR stopband [22].

A Tamm plasmon can be excited with light incident either from the metal side [24], or the DBR side [25]. Ideally, the Tamm plasmon requires both metal and DBR to have a reflectance of 100 %. This is unachievable with realistic metals, although a thick metal layer can have a very high reflectance. A fully reflecting DBR would also require an infinite amount of layers. In reality, high reflectances can be achieved with metal layers of 100 nm thickness or more, and DBR consisting of 9 layers or more, however in order to be excited by incident light, the layer on the incident side needs to be able to transmit light into the confined mode. For light incident on the metal, an efficient coupling to the Tamm plasmon will occur with a metal layer thickness close to 50 nm, and an infinite amount of DBR layers. With light incident from the DBR side a thicker metal layer is better [25].

2.3 Optical resonant cavity

Light can also be confined in an optical cavity consisting of two highly reflective surfaces separated by a transparent spacer layer. Optical cavities are commonly used in several applications, such as interferometers and optical filters. A notable application for cavities is lasers, where stimulated emission is used to amplify the amount of light propagating in the cavity [26]. Light inside the cavity is repeatedly reflected by the mirrors at the ends of the cavity, preventing it from transmitting out of the cavity. The reflections cause the light in the cavity to interfere with itself. At the resonant wavelength of the cavity, the light interferes constructively, causing a standing wave to form in the cavity. Off resonance, the light interferes destructively, causing the reflections to cancel each other out and preventing a wave from forming in the cavity. Due to the strong intensity formed inside the cavity, small amounts of light matching the resonant wavelength is able to escape the cavity, and in the reverse situation, incident light matching the resonant wavelength of the cavity is able to couple in to the cavity.

Because the standing wave forms in the spacing between the mirrors of the cavity, the properties of the spacing layer mainly determine the resonant wavelengths of the cavity. The cavity is resonant at wavelengths equalling the distance of a path back and forth in the cavity,

$$\lambda = \frac{2nd}{m}, \tag{17}$$

where n is the refractive index of the material in the cavity, d is the thickness of the cavity and m is any positive integer. Optical cavities can range in size from several wavelengths long cavities to microcavities with lengths of only a few wavelengths. In this thesis, cavities in which the length matches half of the resonant wavelength, *i.e.*, m equals one in equation 17, will be examined. This creates a standing wave, with only one peak in the electric field, at the middle of the cavity.

Cavities can be manufactured using metallic or dielectric mirrors, or any other reflective surfaces. In this thesis, metallic mirrors are used at both ends of the cavity, with a dielectric material used as spacer. In this case, the resonant cavity forms within the dielectric material that separates the metal layers, allowing light matching the resonant wavelength to couple in to the cavity. This light forms a standing wave between the cavity mirrors, causing strongly enhancement of the electric field at the peak of the standing wave.

Equation 17 assumes that the reflective surfaces at the ends of the cavity are ideal mirrors, in which case the reflected light receives a phase shift equal to π. For metallic mirrors, the phase shift is in reality less than π, causing an increase in the resonant wavelength of the cavity [27]. The resonant wavelength then becomes

$$\lambda = \frac{2nd}{m}\frac{2\pi}{\varphi_1 + \varphi_2}, \tag{18}$$

where φ_1 and φ_2 represent the phase shifts received by the reflected light at each metal-dielectric boundary. The magnitudes of the phase shifts depend on the refractive indices of both metal and dielectric medium and the thicknesses of the metal layers [27]. If the metal layer on either side is nanostructured, it will cause a further increase in the phase shift [28]. Metallic mirrors also absorb and transmit small fractions of the light being reflected, limiting the maximal electric field strength achievable in the cavity.

The highest reflectances, and phase shifts closest to π are achieved by thick metal layers, ideally semi infinite ones. A layer thickness close to 100 nm is enough to confine the electric field very effectively. However, in order to efficiently couple incident light from outside the cavity, the metal layer on the side of incidence needs to be thinner.

One of the goals of this thesis is to investigate the coupling between cavity and plasmonic modes caused by nanostructuring on top of the cavity. There is some evidence of coupling between a cavity and plasmonic structures placed inside the cavity [28]. However, most of the effects from this are located inside the cavity. In this thesis, coupling to structures outside will be investigated, in order to further enhance the near field effects caused by them.

3 Methods

In this thesis, the applicability of different nanostructures designed for electric near field enhancement is examined. The main focus is on simulations of the different types of nanostructures. Based on the simulations, some samples are fabricated and analysed. These samples are compared to the simulated structures by measuring the reflectance spectra of the samples and comparing them to the simulated spectra. Of particular interest are the resonant wavelengths, which are identified by dips appearing in the spectrum of the otherwise reflective samples. The positions and shapes of these dips reveal how well the simulations match the real structures. By examining the electric field at these wavelengths, the nature of the resonant behaviour can be better understood. Due to the dimensions of the structures examined in this thesis being comparable to the wavelength of light, the positions of these dips are strongly affected by relatively small changes in parameters. This can lead to noticeable differences between the simulated and measured spectra, even with structures matching the simulated parameters quite closely, and some differences are expected to be visible in the measurements.

3.1 Simulation

The purpose of a simulation is to create a mathematical construct approximating the behaviour of a real world physical phenomenon. This is achieved by determining the functions and parameters required to accurately model the phenomenon, and making the necessary simplifications in order to get a solvable model. Usually, a simulation includes changing one or more parameters in small discrete steps to observe the behaviour of the system over a range of conditions. The main advantage of simulations is the ability to quickly examine of the behaviour of a system in response to different parameters, without having to fabricate and measure a large number of samples.

Simulations can be either time dependant, or steady state solutions. In a time dependant simulation the system starts at an initial condition, evolving over a range of discrete time steps. Each time step depends on the previous, with the solution of the previous step becoming the initial condition in the next one. In this thesis, steady state simulation is used, which assumes that the response of the simulated system settles to a constant value once a long enough time has passed. Because a continuous excitation with periodic electromagnetic waves is simulated, a steady state solution can be assumed to exist. These waves propagate at the speed of light, causing this solution to be reached almost instantly, and making any time dependent behaviour practically unobservable. The simulations are done in the frequency domain, with solutions acquired for a range of wavelengths. Because the simulation calculates steady state solutions, each solution is independent of the others.

The simulations presented in the result section of this thesis are performed with finite element method (FEM) simulation, using version 5.3 of COMSOL multiphysics software. In FEM, a partial differential equation is solved numerically by dividing the simulated geometry into a set of small elements, and solving the equation in relation to certain points at the edges of the elements, called mesh nodes. The areas between the nodes are described by simple linear or polynomial equations which match with surrounding elements at the at the node positions. This reduces the complexity of the calculation by replacing the partial differential equation with a set of simpler equations, and allows the simulation of complex geometries where no analytical solution to the

partial differential equation exist. These equations do not usually match the partial differential equation perfectly, but instead approximate it closely. The accuracy of this approximation depends on the size of the elements used, and improves as the elements become smaller and the number of elements increases. Acquiring an exact solution would require the use of an infinite amount of elements, and is therefore impossible to achieve. Because the computing power required is directly related to the number of elements used, simulation in practice requires a compromise between solution accuracy and computing time.

The simulation process consists of three main phases: model building, simulation and post processing. The model building phase involves defining the physics necessary for the simulation, and providing instructions for running the simulation. It is the most laborious phase of simulating, but once one model has been made it can usually be used in several different simulations, with slight modifications. In the simulation phase the actual calculations of the simulation are carried out. This is usually mostly done by a computer, and a properly prepared simulation requires no human input at this point. In the post processing phase the large amount of data generated by the simulation is analysed and the relevant information is extracted.

The simulations presented here are carried out in a 2D geometry, which represents a cross section of the structure being investigated. The simulation domain consists of two semi-infinite layers on top of each other, representing air and substrate, with the structure of interest placed between these. The simulation models an infinitely wide structure, by applying suitable periodic boundary conditions at the side edges of the simulation domain. The coordinates used in the simulations follow the convention used in COMSOL for 2D cases, with the horizontal axis defined as the x-axis, with the positive direction to the right, the vertical axis defined as the y-axis with the positive direction upwards, and the z-axis is defined as the axis normal to the simulation plane, with the positive direction inwards.

Simulation in COMSOL starts with choosing the appropriate physics interface, containing expressions for the physical quantities needed in the simulation, as well as the governing equation solved in the simulation. In this thesis the radio frequency interface is used, which uses a time-harmonic wave equation to solve the electric field. This interface allows simulation of electromagnetic waves over a wide range of frequencies, and is well suited for wavelengths in the optical range. The radio frequency interface simulates electromagnetic waves using the electromagnetic wave equation in frequency domain

$$\nabla \times \frac{1}{\mu_r}(\nabla \times E) - k_0^2 \left(\varepsilon_r - \frac{j\sigma}{\omega \epsilon_0}\right) E = 0, \tag{19}$$

where ε_r stands for relative permittivity, ε_0 for vacuum permittivity, μ_r for relative permeability and σ for conductivity. The materials are modelled by their refractive indices, which COMSOL uses to calculate the relative permittivity using the equation

$$\varepsilon_r = (n - ik)^2. \tag{20}$$

In the optical range, μ_r is close to 1 for most materials, and due to the high frequency σ can be assumed as 0. Based on this, the wave equation simplifies to

$$\nabla \times (\nabla \times E) - k_0^2 (n - ik)^2 E = 0. \tag{21}$$

After choosing the appropriate interface, building the simulation model begins by creating the geometry of the simulated domain. Two rectangles, representing air and substrate, are first created on top of each other. The height of the lower rectangle,

representing the substrate, is set to 500 nm. The height of the top rectangle, representing air, is set to 1000 nm. These heights are necessary to allow the near field components to fully decay before reaching the edge. The bottom layer can be quite low due to the low transmittance of the structures simulated here, but in some cases it might be necessary to increase the height of the topmost rectangle. The width of both rectangles is set to equal one period of the simulated structure, when periodic structures are used, or 1000 nm when structures with no periodicity are simulated. The simulated nanostructure is added on top of the boundary between the two rectangles. Each layer of material is represented by a rectangle with width matching the width of the air and substrate layers, and height matching the thickness of the layer. Gratings are created by placing a smaller rectangle, with dimensions matching the grating, on top of a material layer, and removing the boundary between these if necessary. The structure placed this way overwrites part of the upper rectangle, decreasing its actual height, but simplifies modifying the structure if a layer is removed or altered. Figure 3 shows a simulation model of a grating, with the simulation domain containing layers for air and substrate, and a single layer with the grating structure between these. It also shows the same structure with a mesh applied to it.

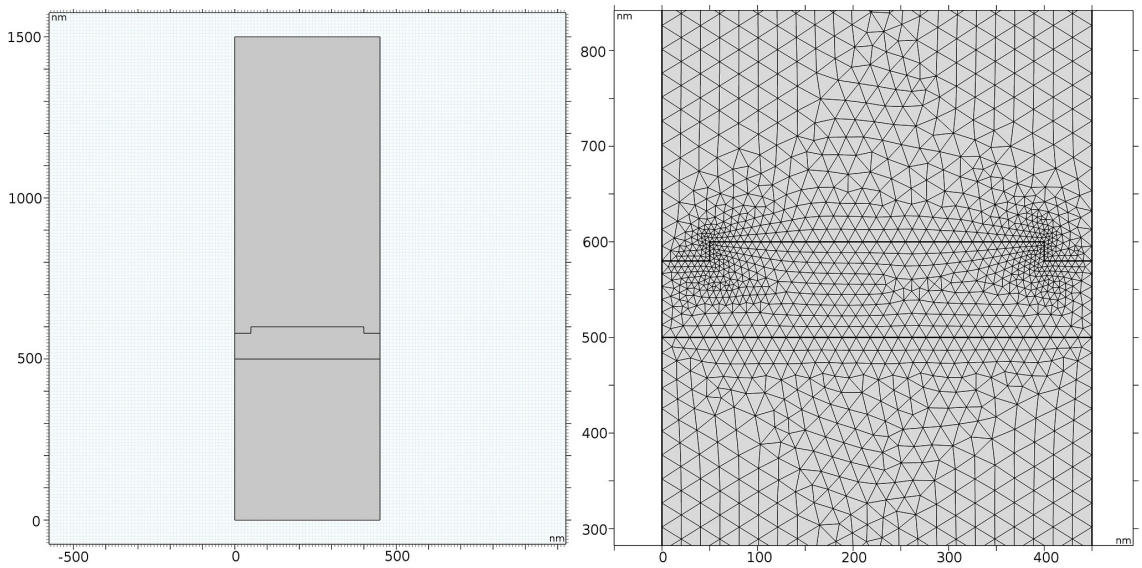

Figure 3: Grating model in COMSOL, representing one period of the actual grating, and the same model with a mesh applied to it. The mesh size at the grating corners is refined to 0.2 times the size of the surrounding mesh.

Next, the different layers of the simulation are given the properties of the materials they represent in the simulation. Each material used in the simulation is defined by giving it the necessary material properties, representing its response to the simulated equation. These materials are then assigned to the appropriate fields in the simulated geometry. In this thesis, the only material parameter used in the simulations is the complex refractive index $\tilde{n} = (n - ik)$. For air the refractive index is assumed to be 1, and for glass 1.52. For the rest of the dielectric materials, the refractive indices are interpolated from measured values, while the values for the metals were taken from reference 29.

The following step is defining the physics for the simulation, and assigning the necessary boundary conditions. The radio frequency interface selected earlier provides the wave equation used in the simulation. The wave equation is solved by dividing the simulated geometry into smaller elements, where the electric field is approximated by

quadratic functions. The wave equation can be solved for only in-plane components of the electric field, for TM polarized waves, or out-of-plane components, for TE polarized waves. The wave equation can also be solved for all three components of the electric field, but this takes significantly more time.

Electromagnetic waves enter and exit the simulation domain through port boundaries. A port is placed on the topmost boundary to input the incident wave and collect the reflected wave. Another port at the bottommost boundary outputs the transmitted wave. The ports are able to output electromagnetic waves matching the shape defined in the port settings, making the domains next to the ports act as a semi-infinite layers. However, any field not matching this shape is fully reflected from the port boundary. Because of this, it is important to make the domains next to the ports thick enough to allow any near field components to fully decay. The top port inputs a plane wave propagating downwards, in the –y direction. This wave can be expressed as

$$E = E_0[Ex, Ey, Ez]e^{-iky}, \tag{22}$$

where Ex = 1, Ey = Ez = 0 for TM polarized light, and Ez = 1, Ex = Ey = 0 for TE polarized light. The input port is fed with 1 W power, which provides an electromagnetic wave with the intensity

$$I_0 = \frac{P_{in}}{A_{port1}}, \tag{23}$$

where A_{port1} is the area of the input port, which in 2D geometry equals to $\text{width} * 1$ m, because COMSOL assumes the depth of 2D objects to be 1 m in calculations. This creates the input electric field

$$E_0 = \sqrt{\frac{2I_0}{n\varepsilon_0 c_0}} = \sqrt{\frac{2P_{in}}{A_{port1} * n\varepsilon_0 c_0}}, \tag{24}$$

where n is the refractive index of the layer next to the port, in this case air, ε_0 is the vacuum permittivity and c_0 is the speed of light. The ports account for the changed angles of reflected and refracted waves, according to Snell's law, but additional port components are needed to deal with diffraction, when simulating periodic gratings. This is done by creating a separate port component for each diffraction order. Periodic boundaries are assigned to the sidewalls of the simulated structures. Floquet periodicity is used, which mimics the effects of an infinitely wide periodic array, by forcing the solution at one boundary to be equal to the opposing boundary, multiplied by a phase shift factor. The magnitude of this phase shift is determined by the component of the wave vector perpendicular to the boundary. Floquet periodicity allows modelling the behaviour of an infinitely wide periodic structure by simulating a single element of the structure. The interior boundaries of the simulation domain do not need to be separately defined, as they are subject to the boundary conditions constraining electromagnetic fields. These conditions state that the electric field component tangential to a boundary and the magnetic field component normal to a boundary need to be continuous.

The final phase of model building is meshing the simulation domain. Meshing is a crucial aspect of FEM simulation, as it determines the accuracy of the solution, and the time required to carry out the simulation. An improperly done mesh can also cause errors in the solution or prevent the solution from converging. Because the number and accuracy of equations in the simulation depends on the number of elements, the size of the elements directly affects the accuracy of the whole solution, and the time required to run the

simulation. It is important to make the mesh fine enough to get a correct solution, but still coarse enough to keep the simulation time reasonable. In the simulations in this thesis, free triangular meshing is used, in which the simulation software attempts to fill the simulation geometry with the least number of triangular elements fulfilling a set of predetermined constraints. The main constraints are maximum and minimum sizes of the elements, and the rates at which elements are allowed to grow or rotate in relation to neighbouring elements. The mesh is a second order mesh, with mesh nodes in the corners and the middle of the sides of the triangles. In order to get an accurate solution from the simulation, a maximum element size of 1/5 of the shortest wavelength is recommended [30]. However, due to the large changes occurring over short distances in the near field in this thesis, a maximum element size of 25 nm, corresponding to 1/12 of the smallest wavelength 300 nm, is used. This size is mainly used in the air and substrate, while the maximum size in the nanostructure layers was reduced to 20 nm. Near sharp corners of the grating, the size is further refined to 0.5 nm, to account for the quickly changing electric fields occurring there. The minimum size parameter is mainly useful to prevent extremely small elements from being created in very complex structures. In this thesis, the structures used are fairly simple, so the minimum size is set to 0.1 nm, which is sufficiently small to not prevent the refinement of the mesh. The maximum growth rate parameter is useful to determine how fast the refined mesh near the corners grows to match the maximum size. This parameter is set to 1.1, which allows the finer area near the corners to extend a sufficient distance. The use of Floquet periodicity in the simulation requires the mesh to be identical at both sidewalls where the periodicity is applied. This is achieved by first assigning the mesh nodes on the boundaries at one sidewall, then copying them over to the other.

Once the simulation domain is fully built and meshed, the simulation can be run. The simulations are done in the wavelength domain, running from 300 nm to 1000 nm, at 1 nm intervals. This provides a sufficient resolution to distinguish the narrow dips in the reflectance spectrum, caused by resonant effects. It is also possible to simulate the angular response, by fixing the wavelength and running the simulation over varying angles. COMSOL also provides the ability to sweep any parameter or set of parameters over a predetermined range, but adding several changing parameters can easily increase the simulation time.

When the simulation has been completed, the acquired solution needs to be post-processed. A simulation can provide a large amount of data, from which the relevant information needs to be extracted and refined into a clear form. Primarily, the reflectance spectrum and the distribution of electric field intensity are examined, while the transmittance spectrum and magnetic field may also be useful. Based on the port boundaries assigned in the model, COMSOL is able to calculate the scattering parameters, or S-parameters, of the system. By defining the incident port as port 1 and the transmitting port as port 2, these can easily be converted to reflectance and transmittance using

$$R = |S_{11}|^2 \; and \; T = |S_{21}|^2. \tag{25}$$

COMSOL also provides expressions for the x-, y- and z-component of the electric field, Ex, Ey and Ez. Using these the electric field intensity relative to the incident field can be calculated. Based on equation 24,

$$I = \frac{E^2 n \epsilon_0 c_0}{2}, \tag{26}$$

where E is the total electric field, *i.e.*, the sum of E_x, E_y and E_z. The intensity relative to the incident field then becomes

$$\frac{I}{I_0} = \frac{|E_x|^2 + |E_y|^2 + |E_z|^2}{E_0^2}. \quad (27)$$

The expression for E_0 was tested by simulating a wave propagating through a 1000 nm * 1000 nm square of air and evaluating $|E_x|^2 + |E_y|^2 + |E_z|^2$. This provides the value $7.545*10^8$ compared to $7.535*10^8$, calculated from equation 24. The relative intensity provides a good estimate of the enhancement of the electric field that can be achieved at different points of the structure, but due to the generalizations in the simulation, these values should not be viewed as fully accurate. Examining the electric field distribution at wavelengths indicated by dips or peaks in the reflectance spectrum provides a quick way to examine the causes of various resonant phenomena.

FEM simulation can be used to efficiently model the behaviour of electromagnetic fields even in very small features, provided a fine enough mesh is used at these points. The ability to visualise both the electric and magnetic field, and solve reflectance and transmittance behaviour of any structure imaginable, provides a valuable asset in designing these structures.

3.3 Sample fabrication

The samples used for the measurements consist of metal and dielectric layers. The samples are fabricated on both glass and Si substrates. Glass is chosen as substrate material due to its cheapness and common use in bioimaging applications. Si substrates are used as reference samples and for measuring the refractive indices of the dielectric materials.

The metals used for the samples in this thesis are mainly gold and silver. In addition to these, a 5 nm thick layer of titanium is used as an adhesion layer between the metals and the glass substrate. This titanium layer is not modelled in the simulations because it has a negligible effect on the electric field enhancement, due to the thick layer of metal on top of it. However, if the surface plasmons occurring on the interface opposite from the incident light were being investigated, this layer would need to be accounted for. The metal layers are deposited by evaporation. In evaporation, the sample is placed at the top of a vacuum chamber. At the bottom, the source material is heated until it evaporates. The evaporated material then rises to the top of the chamber and condenses on the surface of the sample. Vacuum is needed in the chamber to prevent the evaporated material from reacting with other gasses present, and to ensure a uniform layer growth.

Dielectric materials used in this thesis are TiO_2, SiO_2 and TiO2. Atomic layer deposition (ALD) was used to fabricate TiO_2 and Al_2O_3, because of its good thickness control and the uniformity of growth. ALD is able to grow very thin and uniform layers of material. In ALD two precursor gasses are used to grow the material. The precursor gasses are pumped into the chamber one at a time. The gas is allowed to react with the surface, after which the excess gas is pumped out. This leaves a uniform one molecule thick layer attached to the sample surface. After this the second gas is pumped into the chamber, reacting with the surface and the first gas. This cycle is repeated, growing one layer at a time. Because the two precursor gases never mix in the chamber, only the surface of the sample allows the reaction to happen, enabling very good control of growth.

3.4 Measurements

Reflectance measurements are performed through UV-Vis-NIR spectroscopy. The device used for reflectance measurements is an Agilent Cary 5000, with a diffuse reflectance accessory attached to it. The accessory uses a series of mirrors to guide and focus the measurement beam to the sample. During measurements, the sample is placed at the rear wall of an integrating sphere. The integrating sphere consists of a hollow sphere lined with a reflective material, which collects both specular and diffuse reflections and measures them using a photodetector located at the bottom of the sphere. In addition to the measured sample, a high reflectance reference sample is placed at another side of the sphere and constantly measured. The layout of the integrating sphere is shown in figure 4.

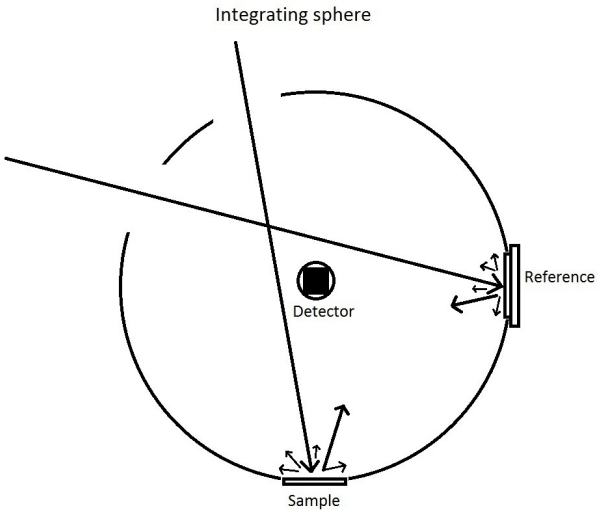

Figure 4: Integrating sphere with slots for the measured sample and a reference sample. The sides of the sphere a lined with a highly reflective material collecting the reflected light from all angles.

The setup of the reflectance accessory is shown in figure 5. The measurement beam is guided by two flat mirrors to a concave mirror, which focuses the beam on the sample placed in the integrating sphere. The reference beam is guided to the reference sample by two mirrors, passing through a focusing lens between the mirrors. The entire setup is housed in a protective casing, which is placed in the accessory slot of the Cary 5000.

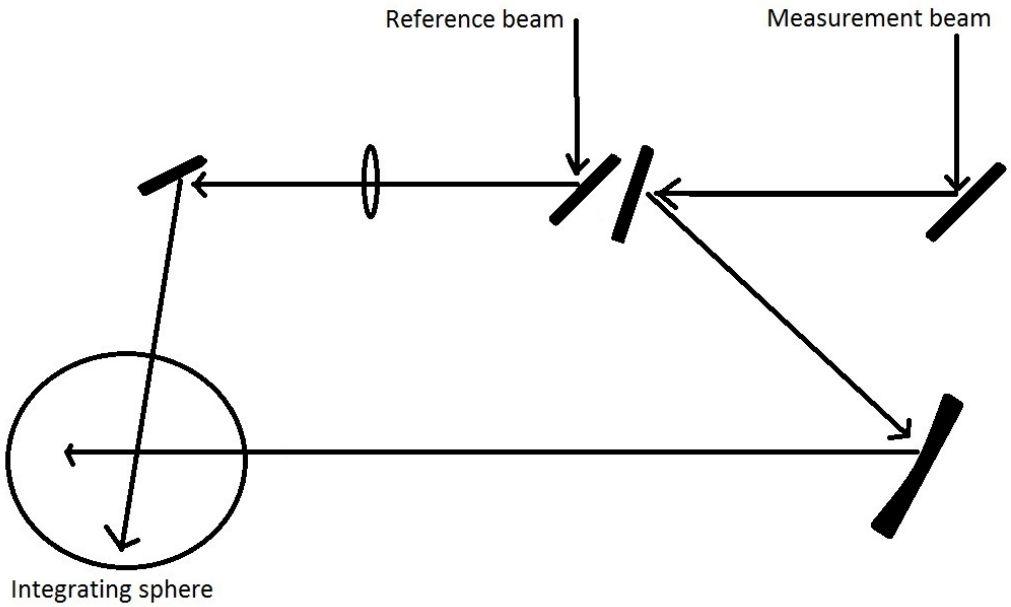

Figure 5: Setup of the diffuse reflectance accessory used for the measurements. The measurement beam is guided by two mirrors to a focusing mirror, which focuses it on the sample placed at the far edge of the integrating sphere. Another beam is guided by two mirrors through a lens, to the reference sample at another edge of the integrating sphere.

Prior to measurements, the device is calibrated by measuring full reflectance from a high reflectance reference sample placed at the sample slot, and by leaving the sample slot empty and measuring the low reflectance background.

A spectral range from 250 – 1000 nm is used in these measurements, with measurements taken at 1 nm intervals. An integration time of 0.1 s is used to measure each wavelength. The reflectance measurements generally provide data of very high quality, although a lamp change at 300 nm and detector change at 800 nm can be seen in some measurements. These are noticeable due to a slight misalignment between the detectors causing the reflectance to sometimes drop at 800 nm and a slight decrease of quality under 300 nm. Luckily these wavelengths are at the edges of the measured spectrum, and do not affect the wavelength region of interest.

The measurement beam allows two modes to be used for its size: full size beam is roughly 0.5 cm wide and 1 cm high, reduced size reduces the height to 0.5 cm. This size is sufficient to measure flat surfaces, and provides a good measure for the average reflectance of the surface. However, this only works for a uniform surface, and in order to examine the uniformity of the surface or measure small features a smaller spot size is needed. Due to fabrication limitations, the grated area of the samples can not be made large enough to cover the spot size, and another measurement setup needs to be constructed in order to be able to measure these structures.

4 Results

In this section the results of the simulations and measurements described in the previous section are presented. First, DBR structures both with and without a metal layer on top are examined, to investigate the effects of the Tamm plasmon and the electric field distribution caused by it. After that, the metal on DBR structure is replaced by a cavity consisting of two metal layers, acting as mirrors, and a dielectric layer between them. The resonant behaviour of this cavity is compared to the Tamm plasmon structure. Next, metallic gratings are used to excite surface plasmons, and the electric fields of these are examined. The effects of the grating and cavity are then combined by applying a grating to the top metal layer on the cavity, in order to examine the interaction between plasmonic modes and resonant cavity modes. Finally, dielectric gratings on plain metal surfaces are investigated.

4.1 Tamm plasmon

A Tamm plasmon is a resonant mode, that can be excited at the interface between a metal layer and a DBR. To examine this phenomenon, DBR structures with and without a gold layer on top are fabricated. The DBR consists of five layers of alternating 85 nm thick TiO_2 and 65 nm thick SiO_2 layers, with the bottommost TiO_2 layer 110 nm thick. Samples are made on both silicon and glass substrates, in order to identify any substrate based effects. Simulations of these samples show reflectance spectra with peaks centred at 570 nm on silicon and 645 nm on glass. The sample on silicon has a reflectance of nearly 80 % at the peak, while the sample on glass achieves a reflectance of 75 %. Because the DBR consists of only 5 layers, the achieved reflectance is not very high, and the shape of the reflectance peak is quite round, rather than the flat peak typical for DBR with higher numbers of layers. Figure 6 shows the measured and simulated spectra of both the silicon and glass sample. The measured spectrum for the silicon sample matches the simulated one quite well, but the sample on glass substrate shows a clear difference between measurement and simulation. This behaviour can be observed in many of the samples examined for this thesis, with the sample fabricated on silicon usually matching the simulated one much better than the one on glass. One possible explanation for this behaviour is a difference in the growth rate and refractive index of materials grown on the different substrates. This would lead to a difference in the optical thickness of the material layers on the two substrates, causing differing optical behaviour. Because the refractive indices and layer thicknesses are measured only on the silicon sample, this could cause the silicon samples to match better with the simulation. It is also noticeable that the simulated spectra of the two samples in this case differ from each other quite a lot, suggesting that the substrate has a significant effect on the reflective behaviour of the overall structure. This is caused by the DBR structure transmitting a significant amount light to the substrate, and increasing the reflectance of the DBR, by increasing the number of layers, should lessen the difference.

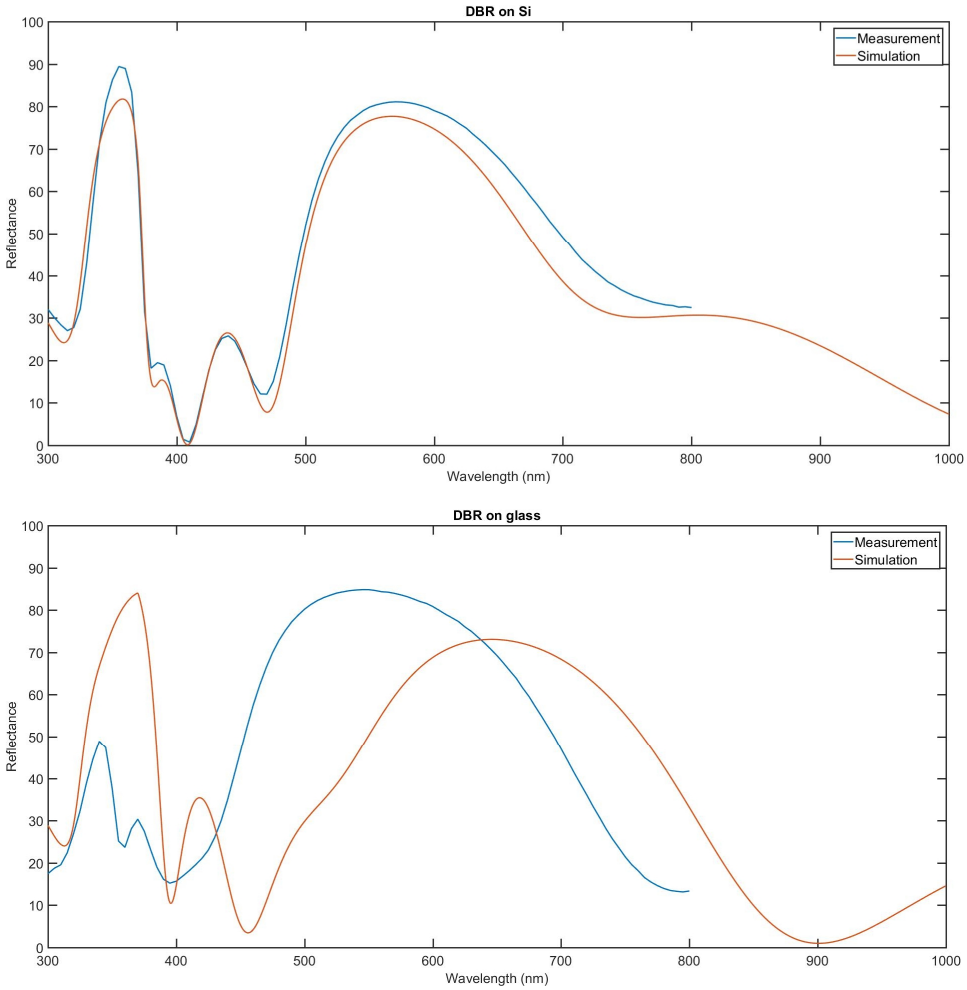

Figure 6: Measured and simulated reflectance spectra of DBR on Si and glass substrates. The sample on Si shows good agreement between the simulation and measurement, while the measured sample on glass diverges more from the simulation.

The high reflectance of the DBR is caused by constructive and destructive interferences, due to the reflections from every interface being in phase with each other in the reflecting direction, and out of phase in the transmitting direction. Figure 7 shows the simulated electric field distribution in the sample fabricated on silicon substrate at the peak reflectance at 567 nm and at the dip occurring at 470 nm. At maximum reflectance, the electric field forms a standing wave in the DBR, with a field minimum and maximum coinciding at alternating boundaries, except the last boundary where the layer thickness is higher. The electric field gets gradually weaker, deeper in the structure. The image also shows a strong electric field maximum slightly above the first interface, between air and TiO_2. This maximum is caused by the high reflectance of the DBR creating a standing wave in the near field. This kind of standing wave is formed above all reflective surfaces, and can also be observed in many of the later simulations. For an ideal mirror, the standing wave should achieve an intensity four times the incident one. Because the DBR is unable to fully reflect the light, the standing wave only reaches an intensity of 3.55.

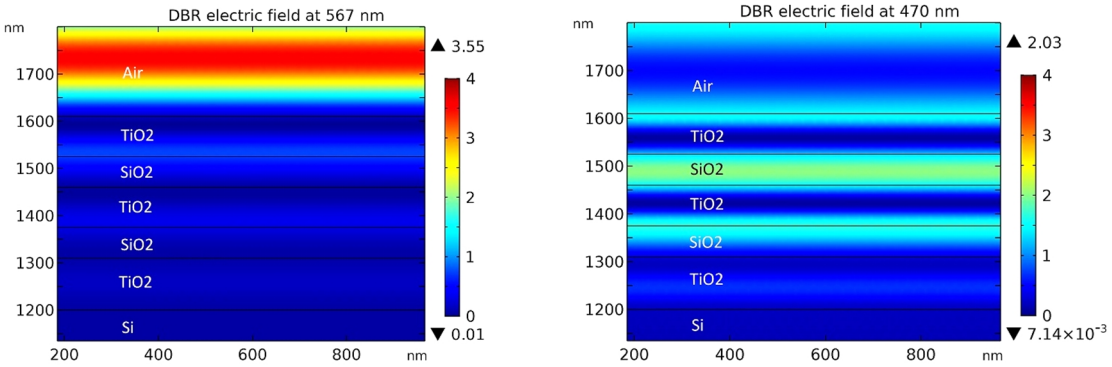

Figure 7: Electric field intensity distribution at the reflectance peak at 567 nm and the dip at 470 nm, in the DBR fabricated on silicon substrate. At the reflectance peak, the electric field in the DBR is very weak due to destructive interference in the structure. The high reflectance creates a standing wave outside the structure, close to the surface. At the reflectance minimum, a much stronger electric filed is visible in the DBR, indicating a higher transmittance.

At the reflectance minimum, much more light is able to transmit through the structure, causing a much stronger electric field inside the DBR. The wavelength is noticeably lower than twice the thickness of TiO_2 and SiO_2, causing the electric field minima and maxima to not align with the layer boundaries. At the maximal reflectance, the first interface of the DBR contains an electric field minimum, whereas the image from the reflectance dip shows a maximum occurring at the first interface.

By depositing a 50 nm thick layer of gold on top of the above DBR, a Tamm plasmon structure is created. The reflectance of this structure mostly matches the reflectance of the gold layer, except for a dip at the resonant wavelength of the structure indicating coupling to the confined mode. In this case, a very small dip is visible in the reflectance spectrum at 690 nm on the silicon substrate, as shown in figure 8, and 595 nm on the glass substrate. Again, the sample on silicon matches the simulation quite well, while the sample on glass matches it more poorly. As expected, the dip in reflectance occurs at a wavelength slightly above the wavelength for maximum of the DBR.

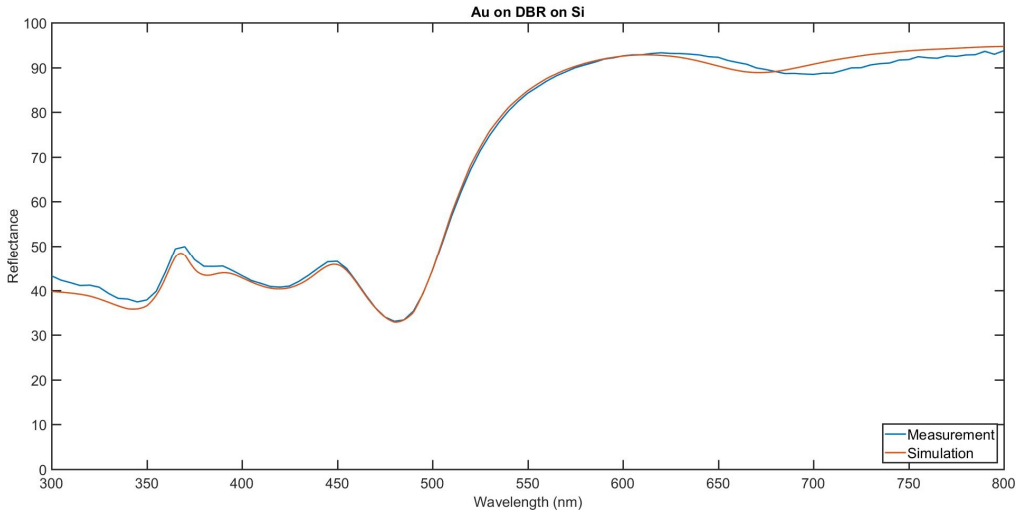

Figure 8: Reflectance spectrum of a DBR covered by gold, fabricated on a silicon substrate. A slight dip is visible at 690 nm, indicating coupling to the Tamm plasmon. This dip is very shallow, indicating a weak coupling.

As can be seen in the figure, the dip appearing in this structure is very shallow and wide, indicating very weak coupling to the resonant mode. In a case with efficient coupling to a resonant mode, a sharp and narrow dip is expected. The poor coupling mainly is caused by the five layers of the DBR being insufficient to contain the resonant mode properly, and thereby also preventing efficient coupling. By increasing the amount of layers to correspond to a reflectance closer to 100 %, the coupling efficiency should improve.

The coupling efficiency is also affected by the thickness of the gold layer on top of the DBR. If the metal layer is too thin, it will allow a large portion of the incident light to simply transmit through the metal, and get reflected by the DBR, increasing the reflectance at the resonant wavelength, and moving the resonant wavelength slightly higher. A too thick metal layer will also increase reflectance by simply reflecting most of the incident light at the boundary between air and metal, hindering coupling into the structure entirely. This sample also transmits much of the coupled light at the resonant wavelength, causing the electric field inside the structure to remain very weak at resonance, as figure 9 shows. The electric field maxima and minima also occur close to the middle of the layers, instead of aligning with the interfaces between TiO_2 and SiO_2, suggesting the condition for constructive interference in the DBR is not fulfilled properly. This is due to the poor confinement in the five layer DBR structure allowing much of the field inside the structure to transmit out, preventing a strong interference. Adding more layers to the DBR would also reduce the transmittance at the resonant wavelength and improve the confinement of the electric field, but due to the electric field intensity growing very high at better a confinement, a large number of layers would be needed to decrease transmittance sufficiently. Adjusting the thicknesses of the TiO_2 and SiO_2 layers changes the position of the DBR reflectance peak, and thereby also the resonant wavelength of the DBR covered by a gold layer.

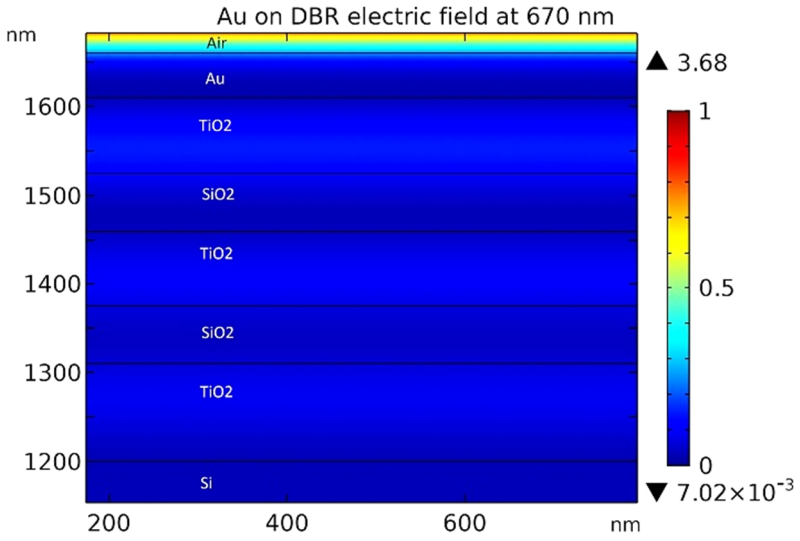

Figure 9: Electric field inside Au covered DBR structure at the resonant wavelength. In this case the coupling is very poor and the electric field in the structure remains weak.

In order to examine the Tamm plasmon under more efficient coupling, a DBR structure with the amount of layers increased to nine is simulated. The layer thicknesses are also adjusted to 70 nm for TiO_2 and 100 nm for SiO_2, which is close to equal optical

thickness, making both layers roughly a quarter wavelength thick at resonance. This DBR is simulated on glass substrate, to eliminate any effects caused by reflections from silicon. The reflectance spectrum, shown in figure 10, shows the DBR has a peak in the reflectance at 616 nm, with a peak reflectance over 95 %. The top of the reflectance peak is flatter than in the five layer DBR, and the reflectance drops sharper, forming a distinctive optical band edge. Like in the previous five layer DBR, the electric field, shown in figure 11, has a minimum and maximum located at alternating boundaries. In this case, the electric field also clearly gets weaker at each subsequent maximum, due to the decreasing amount of light transmitted to the next layer. Adding a 50 nm thick layer of gold on top of this DBR structure forms a dip in the reflectance spectrum at 704 nm. Now the dip is much deeper than in the previously measured case, and is clearly distinguishable in the spectrum. The reflectance at the resonant wavelength drops below 25 %, indicating a fairly strong coupling to the resonant mode. However, the transmittance spectrum also reveals a strong peak at the resonant wavelength, with a transmittance higher than 50 %. This is significantly higher than the transmittance of the gold layer or DBR alone, suggesting that the resonant coupling allows more light to couple into the structure than it is able to contain. With the high transmittance, only a little more than 25 % of incident light is actually contained in the structure, while the rest is either reflected or transmitted. The electric field at this wavelength shows a maximum at the first TiO_2-SiO_2 interface, with an enhancement of 4.85. This is slightly more than the maximum from a standing wave near a perfect reflective surface, suggesting that the gold covered DBR can be used to enhance the electric field inside the structure. Contrary to some descriptions about the Tamm plasmon, no surface wave is observed in these simulations, suggesting that the resonant behaviour is entirely caused by reflections between the gold layer and DBR, similar to an optical cavity.

The likely cause for the high transmittance in this structure is the resonant wavelength being slightly higher than the wavelength for maximum reflectance of the DBR, causing the resonant dip to occur at the edge of the DBR stopband. While the reflectance of the DBR structure by on its own is still 90 % at this wavelength, the enhanced electric field causes an increase in the transmittance. According to equation 15, the reflectance peak of the DBR is centred on the wavelength $\lambda_0 = 2(n_1 d_1 + n_2 d_2) = 616$ nm, which is twice the optical thickness of the two materials. When a gold layer is added on top of this structure, the reflectance of the gold creates a confined mode between the two reflective surfaces, according to [22], which should depend on the reflectance behaviour of the DBR. However, due to a phase shift occurring on reflection from the gold surface, caused by the wave penetrating a small distance into the metal, the resonant wavelength shifts to a slightly higher wavelength above the reflectance peak. Similarly to the case of a cavity, described in equation 18, the resonant wavelength becomes

$$\lambda = 2 * (n_1 d_1 + n_2 d_2) * \frac{\pi}{\varphi} = 704 \text{ nm}, \tag{28}$$

where the phase shift on reflection from an ideal mirror is π, while the phase shift caused by reflection from the gold surface is φ. In fact, these simulations suggest that the resonant confinement in the gold covered DBR is based on the same effect as in an optical cavity. While in a conventional cavity, the resonant mode forms in a spacer layer placed between two reflective surfaces, in the gold covered DBR it appears to form in the first pair of TiO_2 and SiO_2 instead. Because the gold is placed directly on the topmost TiO_2 layer, the topmost interface does not act as a reflective surface, and causes the topmost two layers to instead act similarly to a spacer. Due to the two layers having the same

optical length, the peak of the standing wave occurs at the boundary between them, which is at the centre of the cavity.

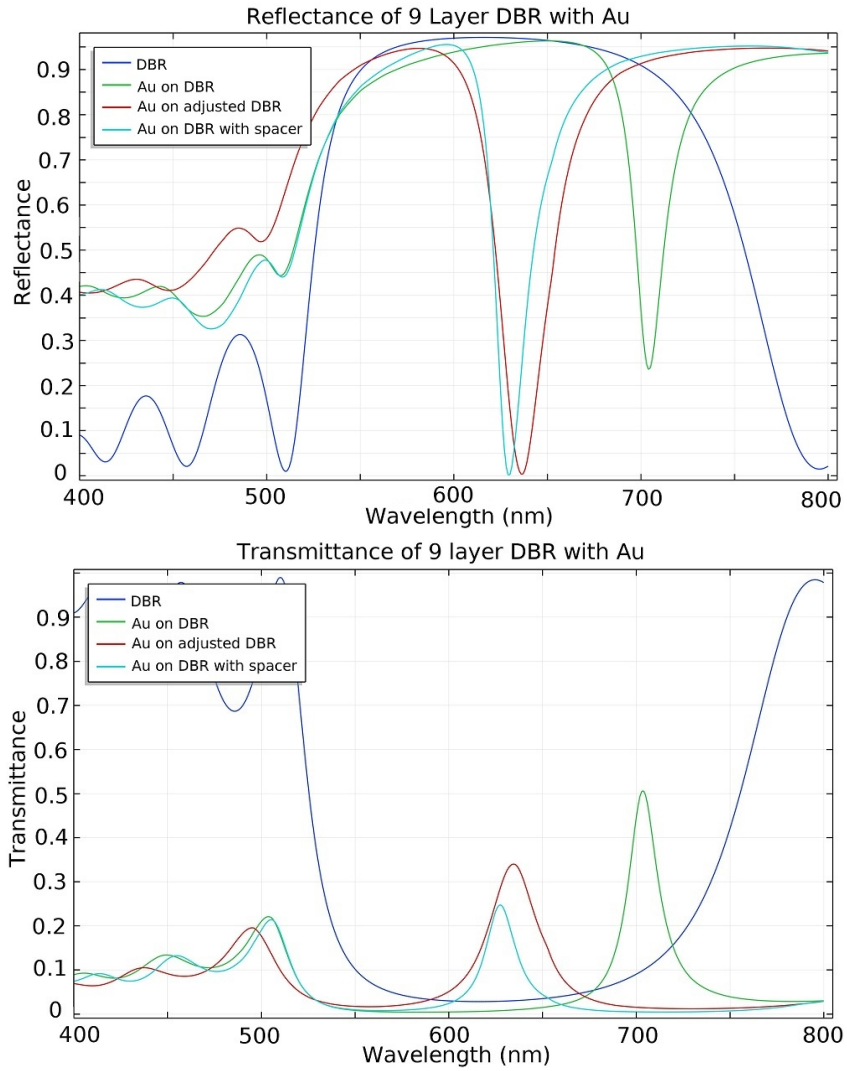

Figure 10: Reflectance and transmittance spectra of the bare DBR, DBR with a gold layer on top, DBR with reduced top layer thicknesses with gold on top and DBR and gold with a spacer layer between. The two modified structures exhibit both lower reflectance and transmittance, suggesting the coupling efficiency of the gold covered DBR can be enhanced by moving the resonant wavelength closer to the centre wavelength of the DBR.

To counteract this phase shift, two solutions are tested. First, the thicknesses of the two topmost layers of the DBR are reduced to 50 nm for TiO_2 and 80 nm for SiO_2. This should reduce the length of the cavity, moving the resonant dip closer to the DBR reflectance maximum. Secondly, a 180 nm thick SiO_2 spacer layer is added between the gold layer and DBR, forming a conventional cavity structure matching the reflective wavelength of the DBR. As can be seen in figure 10, both structures move the resonant wavelength to 630 nm, close to the reflectance peak of the DBR. In both cases the reflectance drops to almost 0 % at resonance. The transmittance is also significantly reduced, to 34 % for the DBR with adjusted top layers, and 25 % for the DBR with the spacer. The lower transmittance in the DBR with spacer is probably caused by moving the first TiO_2 layer away from the gold layer, causing an additional reflective interface to

appear, and making the DBR effectively have an additional pair of layers. In order to get the transmittance further reduced, more layers would need to be added to the DBR. However, the effectiveness of each added layer is likely reduced by the stronger electric field causing higher transmittance, as evidenced by all transmittances being higher than that of the bare DBR.

The electric field distributions at the resonant wavelengths, seen in figure 11, show that the two structures also further improve the enhancement of the electric field in the structure. The structure with the thicknesses of the top layers reduced has a maximal electric field intensity 7.48 times that of the incident field, while the structure with the spacer between gold and DBR shows an electric field enhancement of 15.5. This suggests that a conventional cavity may be more effective at providing electric field enhancement than the gold covered DBR. The two modified structures also show an electric field distribution similar to the bare DBR, with electric field minima and maxima coinciding with every second material interface, while the unmodified gold on DBR structure show a slight offset from these positions.

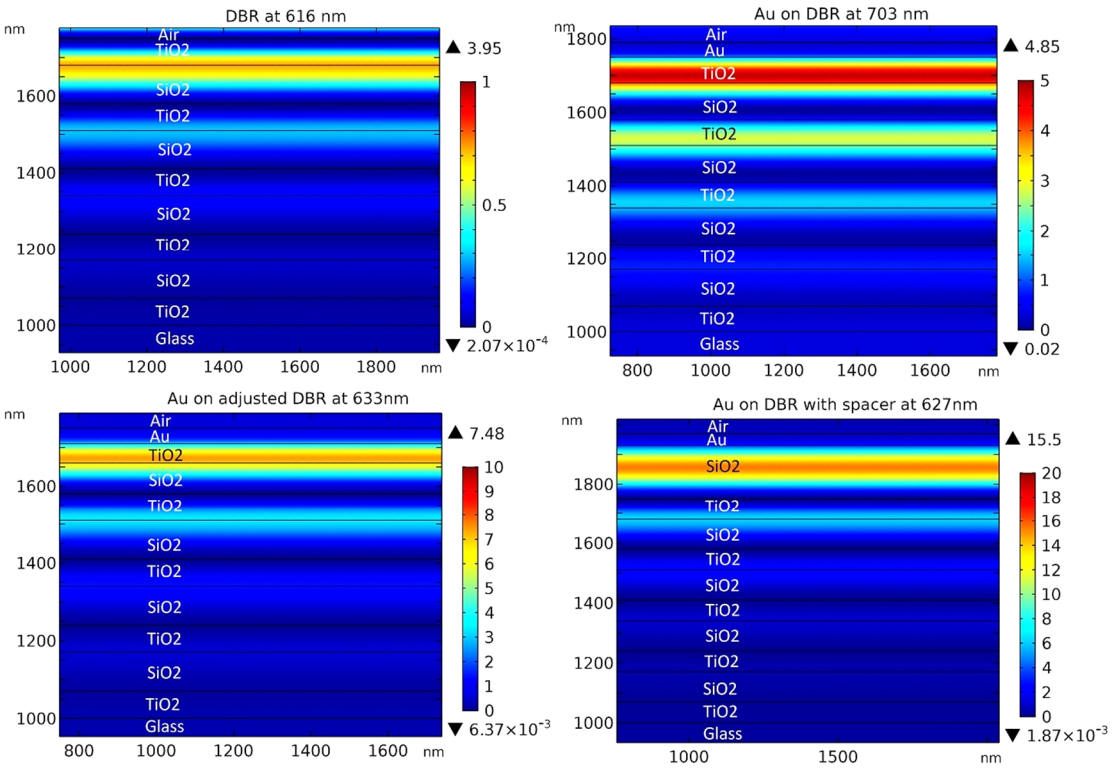

Figure 11: Electric field intensity in DBR, Au on DBR, Au on DBR with adjusted top layers and Au on DBR with spacer between, at resonant wavelength. The positions of the electric field maxima in the two modified structures closely match those of the bare DBR, while the unmodified Au on DBR displays a slight offset from this. Of these four structures, the one with a spacer layer forming a conventional cavity clearly provides the highest electric field enhancement.

4.2 Optical cavity

Instead of using a DBR, an optical cavity can be created by simply placing two reflective metal layers on both sides of a dielectric spacer layer. In this case, the two metal layers

act as mirrors, confining light between them through multiple reflections. The light reflecting back and forth between the metal layers interferes constructively, causing a standing wave to be formed at the resonant wavelength. At other wavelengths, no light can propagate in the cavity due to destructive interference. As shown in section 2.3, a cavity is resonant at wavelengths where the optical thickness of the cavity equals a multiple of half the wavelength. As with the DBR case, the reflections from the gold surfaces cause phase shifts unequal to π, which increase the effective length of the cavity. In the metal cavity, this effect doubles, due to there being two metal interfaces. With suitable thicknesses of the metal layers, light incident on the cavity, matching the resonant wavelength, is able to couple into the cavity, while other wavelengths will get reflected.

A cavity structure consisting of 40 nm thick gold layers separated by 50 nm of TiO_2 is examined. This structure is resonant at 530 nm. As previously, the sample on silicon substrate matches well with the simulation, while the sample on glass substrate differs a bit. The reflectance spectrum of the structure on silicon is shown in figure 12. A dip can be seen in the reflectance at the resonant wavelength, similar to the gold covered DBR. One edge of the dip is considerably lower than the other, because the reflectance of gold starts to drop at 550 nm. The lowered reflectance of gold at short wavelengths is caused by increased absorption by the gold. This limits the efficiency of gold at lower wavelengths, because the electric field enhancement in the cavity depends on the metal being highly reflective.

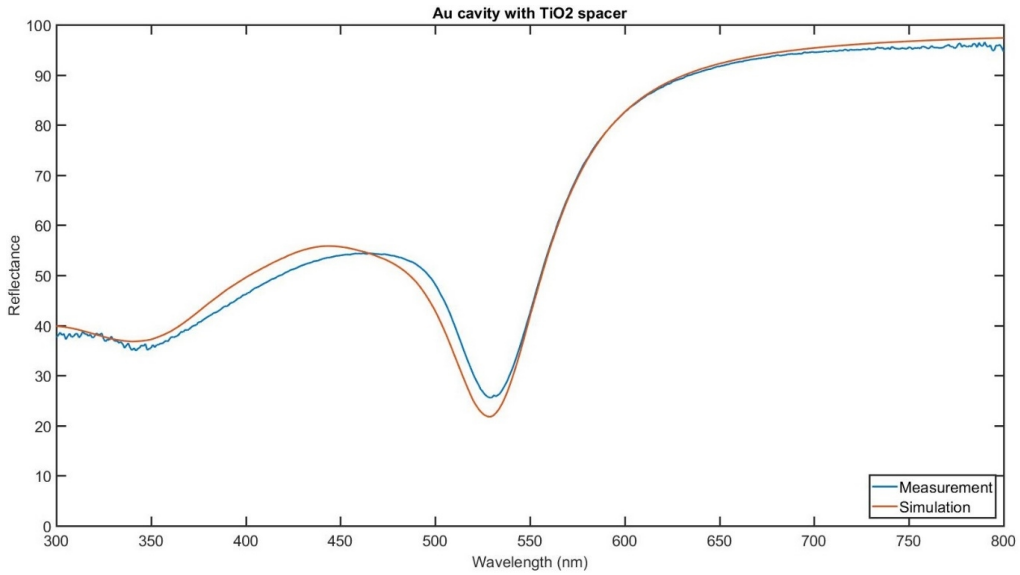

Figure 12: Measured and simulated reflectance spectra of a gold cavity with TiO_2 spacer on a Si substrate. The resonant wavelength is 530 nm.

Figure 13 shows the electric field in the cavity at the resonant wavelength. The electric field inside the cavity is not very strong, barely matching the intensity of the input field. This weak electric field suggests that the lowered reflectance of gold is already affecting the efficiency of the structure. The electric field in the top gold layer is also noticeably higher than in the bottom layer, due to light transmitting through the top layer. This also causes the electric field maximum to be located slightly above the middle of the cavity.

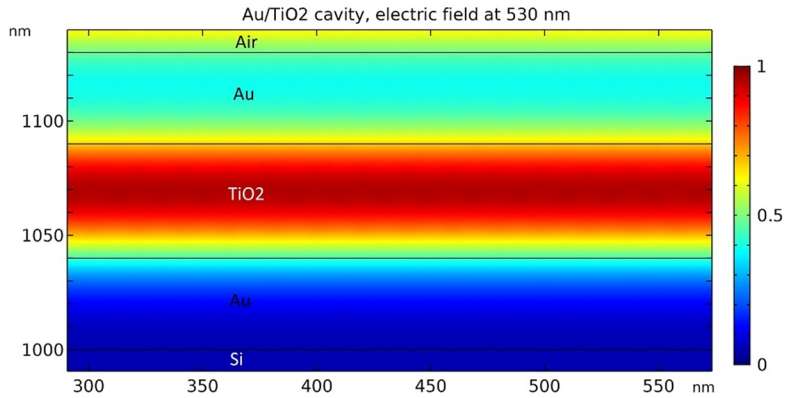

Figure 13: Electric field in the gold cavity with TiO_2 spacer at the resonant wavelength. The electric field intensity in the cavity is barely equal to the incident light, and the electric field in the top most gold layer is noticeably higher than in the bottommost layer.

In order to have the cavity work efficiently at wavelengths close to 500 nm, the gold layers are replaced with silver. As shown in section 2.1, silver stays highly reflective at wavelengths down to 350 nm. However, silver oxidizes more strongly than gold, requiring a protective layer between silver and air. In this case, a thin layer of the dielectric used in the cavity can be deposited on the topmost silver layer. To examine the silver cavities, cavities consisting of a 57 nm thick TiO_2 layer between 40 nm thick layers of silver are fabricated. Surprisingly, the sample fabricated on glass now matches the simulation quite well, while the one on silicon differs more. This could be caused by the change from gold

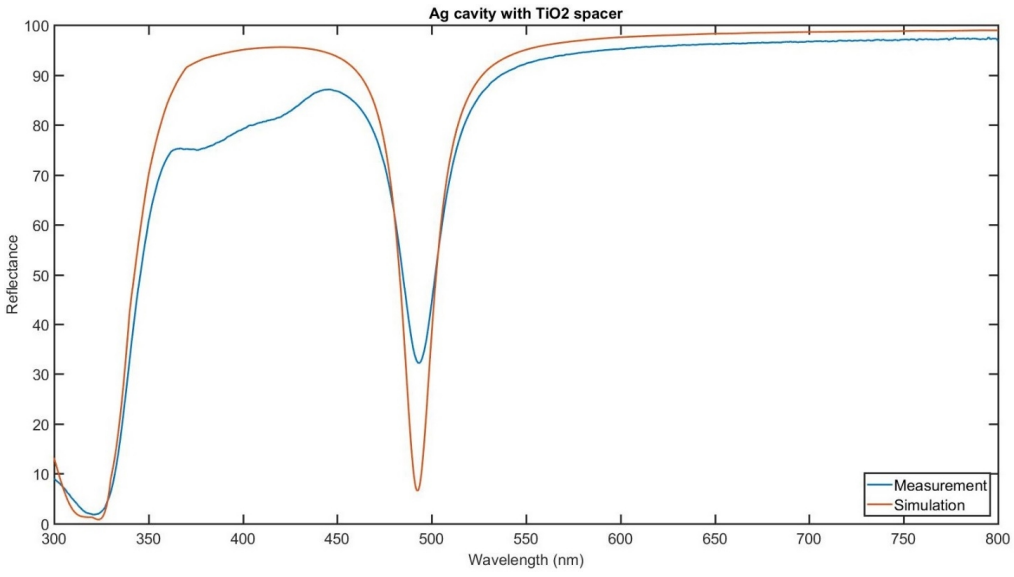

Figure 14: Measured and simulated reflectance spectra of a silver cavity with TiO_2 spacer, on a glass substrate. The positions of the dips match each other well, but there is a large difference in the reflectance at resonance. The measured sample also shows an anomaly between 350 nm and 450 nm.

to silver, as the different metals can have different surface characteristics, affecting the growth conditions of the TiO_2 layer. Figure 14 shows the reflectance spectrum of the

cavity sample on a glass substrate. A stronger dip is now visible at 495 nm. While the position of the dip matches the simulation quite well, the reflectance of the measured sample is almost 25 % higher than the simulation at the resonant wavelength. This is likely either due to the thicknesses of the metal layers in the sample differing slightly from 40 nm, or the refractive index differing from the values used in the simulation. In either case, the metal thickness differs from the optimal, which weakens the coupling efficiency into the resonant mode, increasing the reflectance. The reflectance spectrum also noticeably differs from the simulated spectrum between 350 and 450 nm, showing two slight dips. This might be caused by oxidation of silver during the deposition of the TiO_2 layer.

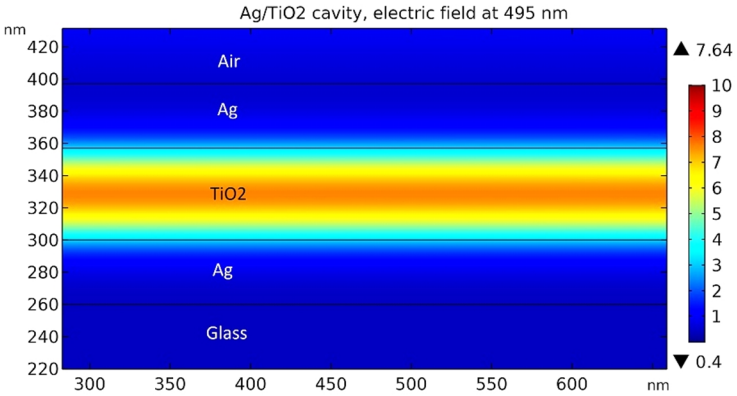

Figure 15: Electric field in the Ag cavity with TiO_2 spacer. The electric field is clearly enhanced in the cavity, but the enhancement remains quite low.

Figure 15 shows the electric field in this structure. The field is now more efficiently confined in the cavity, providing an enhancement of 7.64. This is much better than the gold cavity, but still weaker than in the cavity with DBR. The main reason for the enhancement remaining quite weak is high transmission through the bottom metal layer. The simulated transmittance spectrum, shown in figure 16, has a strong peak at the resonant wavelength, showing a transmittance over 60 %. This indicates that the 40 nm layer at the bottom of the cavity is insufficient to fully contain the resonant mode, and the thicknesses of the metal layers need to be adjusted for the cavity.

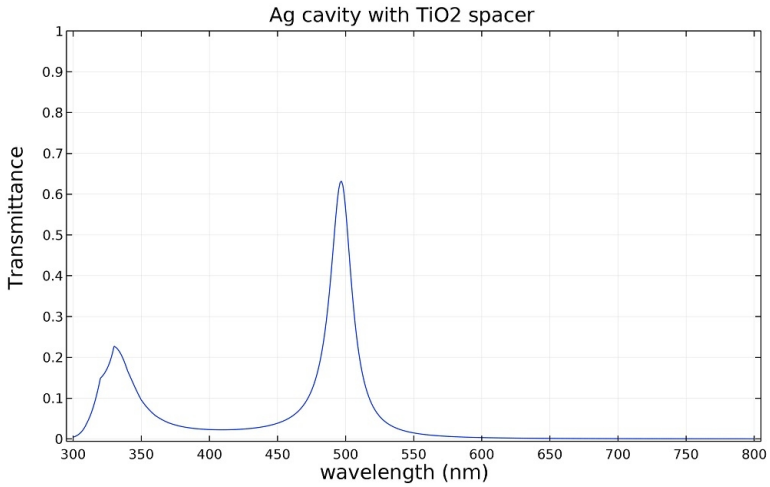

Figure 16: Simulated transmittance spectrum of the cavity consisting of 40 nm thick Ag layers separated by 57 nm of TiO_2. At the resonant wavelength, most of the incident light gets transmitted through the structure

In order to optimize the confinement in the cavity, the top metal needs to be relatively thin, to allow incident light to transmit into the cavity, but the metal at the bottom should optimally be as thick as possible. The thickness of the spacer layer does not affect the optimal thickness of the metal layers, but the refractive index does have a very small effect. A higher refractive index of the spacer causes the wave to penetrate slightly more into the metal, requiring slightly thicker metal layers. The optimal thicknesses of the metal layers also depend on the resonant wavelength, as longer wavelengths propagate deeper into the metal. At 500 nm, a cavity with a 50 nm thick silver layer on the top and an 80 nm thick silver layer at the bottom of the cavity, will provide the best confinement. The dielectric material in the cavity is a changed to Al_2O_3, in order to reduce the oxidation of silver. The thickness of the Al_2O_3 layer is set to 108 nm, which provides a resonant wavelength slightly below 500 nm. Due to the increased thickness of the bottom metal layer, the simulated spectra for samples on silicon and glass substrates are almost identical. The measured spectra, however differ slightly, with the resonant dip occurring at wavelengths 15 nm apart, the sample on glass now being closer to the simulated. All of these spectra have been plotted in figure 17.

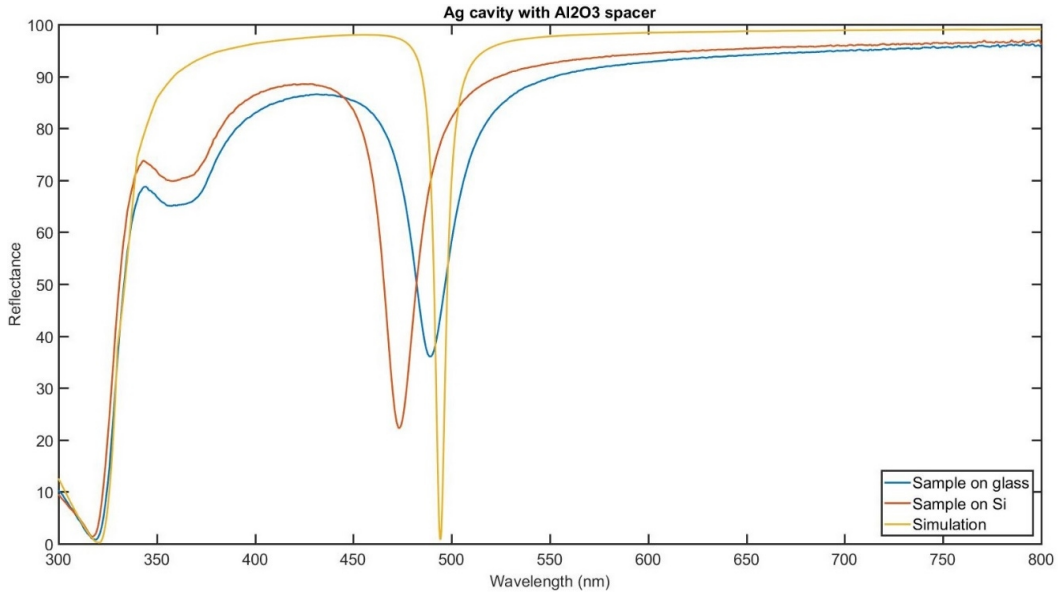

Figure 17: Reflectance spectra of Ag cavity with Al_2O_3 spacer fabricated on glass and Si, and the simulated spectrum.

Similarly to the samples with TiO_2 spacer, an anomaly can be observed around 350 nm. This anomaly exists in both of the measured samples, but differs from the one in the TiO_2 samples, suggesting it is related to the spacer material but not the structural parameters. The transmittance spectrum, shown in figure 18, shows that the transmittance in this sample is significantly reduced, to less than 10 %, at the resonant wavelength. As can be seen from the electric field image shown in figure 19, this creates a sufficient confinement to enable an electric field enhancement of almost 50 to form in the cavity. This could be improved to slightly over 50, by making the bottom metal layer even thicker.

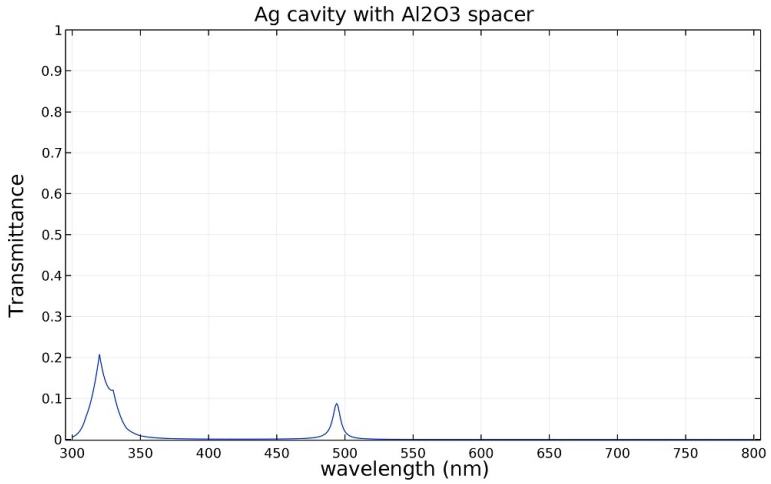

Figure 18: Simulated transmittance spectrum of cavity consisting of 108 nm Al_2O_3 spacer with 50 nm Ag on top and 80 nm Ag on the bottom. The transmittance at the resonant wavelength is now less than 10 %. The higher peak at 320 nm corresponds to the lowered reflectance of Ag at that wavelength.

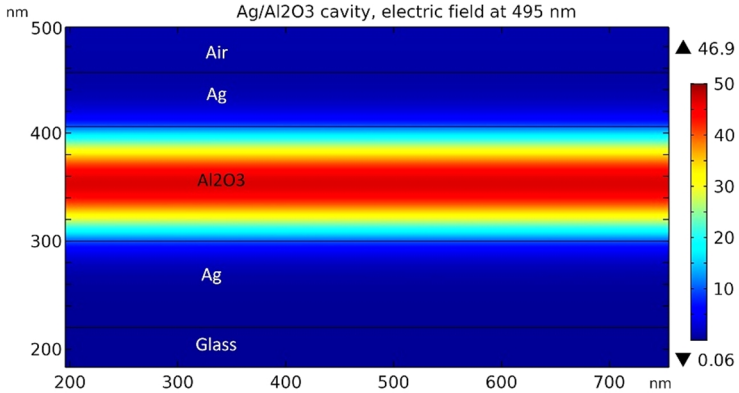

Figure 19: Electric field inside Ag cavity with Al_2O_3 spacer. The electric field intensity in the cavity is now close to 50 times the incident intensity.

The effect of different top layer thicknesses on the cavity is shown in figure 20. It is clear that there exists an optimal thickness of the top layer, in this case close to 50 nm, where the incident light is fully coupled to the cavity. Thicknesses below this will cause the resonance to get weaker, and shift the resonant wavelength higher. This is caused by the thinner metal layer being unable to fully contain the electric field, causing the effective length of the cavity to extend outside the metal. With a metal layer thicker than optimal, the resonant wavelength remains the same, but the coupling strength gets weaker. The bottom layer thickness in this case is 80 nm, increasing it does not have a significant effect on the spectra.

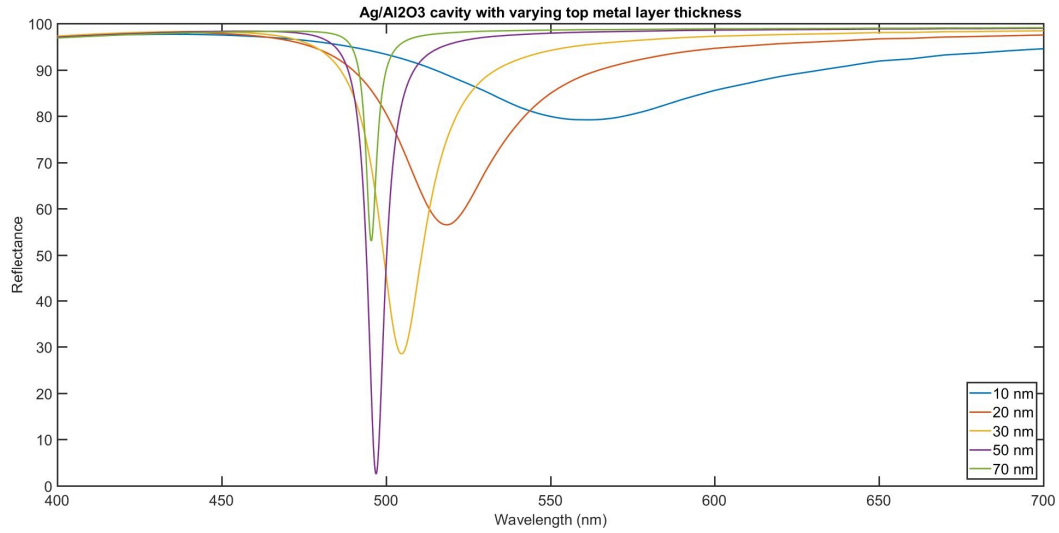

Figure 20: Simulated reflectance spectra for cavities with varying thickness of the top Ag layer. An optimal thickness is found close to 50 nm, where the reflectance drops to zero. With thicknesses thinner than optimal, the resonant wavelength moves higher.

In order to determine the angular dependence of the resonant dip position, a series of simulations with varying angles is carried out. The results, for both TE and TM polarized light, are plotted in figure 21. At normal incidence both polarizations are resonant at the same wavelength, but at higher angles they start to differ. The resonant wavelength decreases as the angle increases, for both polarizations, but for TE polarized light it does so at a faster rate, leading to a 60 nm difference in the resonant wavelength for TE and TM polarized light at grazing incidence. This result is in good agreement with results reported in reference 27.

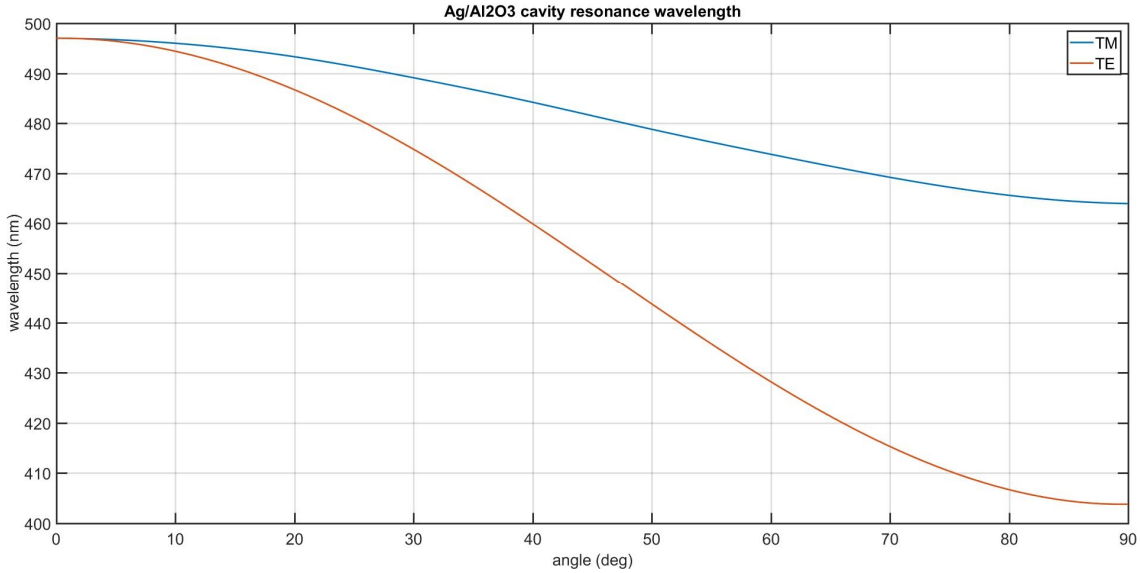

Figure 21: Resonant wavelength for an Ag cavity with Al_2O_3 spacer at varying angles for TE and TM polarized light.

4.3 Metal gratings

Next, surface plasmons excited by metallic gratings are examined. This is mainly done through simulations, in order to examine the electric field distribution caused by different structures. Because the target wavelength is around 500 nm, silver is used instead of gold. Gratings are able to excite surface plasmons both on top of the grating, and on the interface opposite from the grating. Because only the surface plasmons on top of the grating are of interest here, a thick silver layer is used. This provides a high reflectance, enhancing the plasmons on the top and weakening the plasmons below the metal layer. An 80 nm thick silver layer is used in the simulations, with the grating structure placed on top of it. All simulations are performed with TM polarized radiation, as TE polarization does not produce any plasmons.

Figure 22 shows the reflectance spectra and electric field distributions of three metallic gratings, with varying parameters. The grating period for all of these is fixed at 440 nm. The first grating consists of 20 nm high gratings, with a grating width of 340 nm, leaving a 100 nm wide spacing between grating elements. This structure has a strong resonant dip at 496 nm, indicating efficient coupling to the surface plasmon mode. At the resonant wavelength, the electric field is greatly enhanced directly on top of the grating. The electric field at this wavelength consists of a strong enhancement localized at the grating corner, paired with a lesser enhancement on top of the grating, close to the corners, extending 100 nm from the grating surface. In the second grating the grating width is reduced to 240 nm. This causes the coupling to surface plasmons to get slightly weaker, as shown by the lesser dip, and the resonant wavelength to shift a few nm lower. The electric field enhancement is as strong as in the previous grating, but it is more localized to the corners. Changing the spacing of the grating does not seem to have a very large effect on the surface plasmon. In the third grating, the spacing of the second grating is preserved, and the height of the grating is increased to 50 nm. This causes the resonant wavelength to shift higher, to 530 nm, and also causes the dip to get considerably weaker. The effect on the reflectance spectrum is similar to lowering the thickness of the top layer of a cavity, suggesting the weakened coupling is likely caused by a decreased ability to contain the surface plasmon. The electric field is now strongly localized to the grating corners, and the enhancement is less than half of that in the previous gratings.

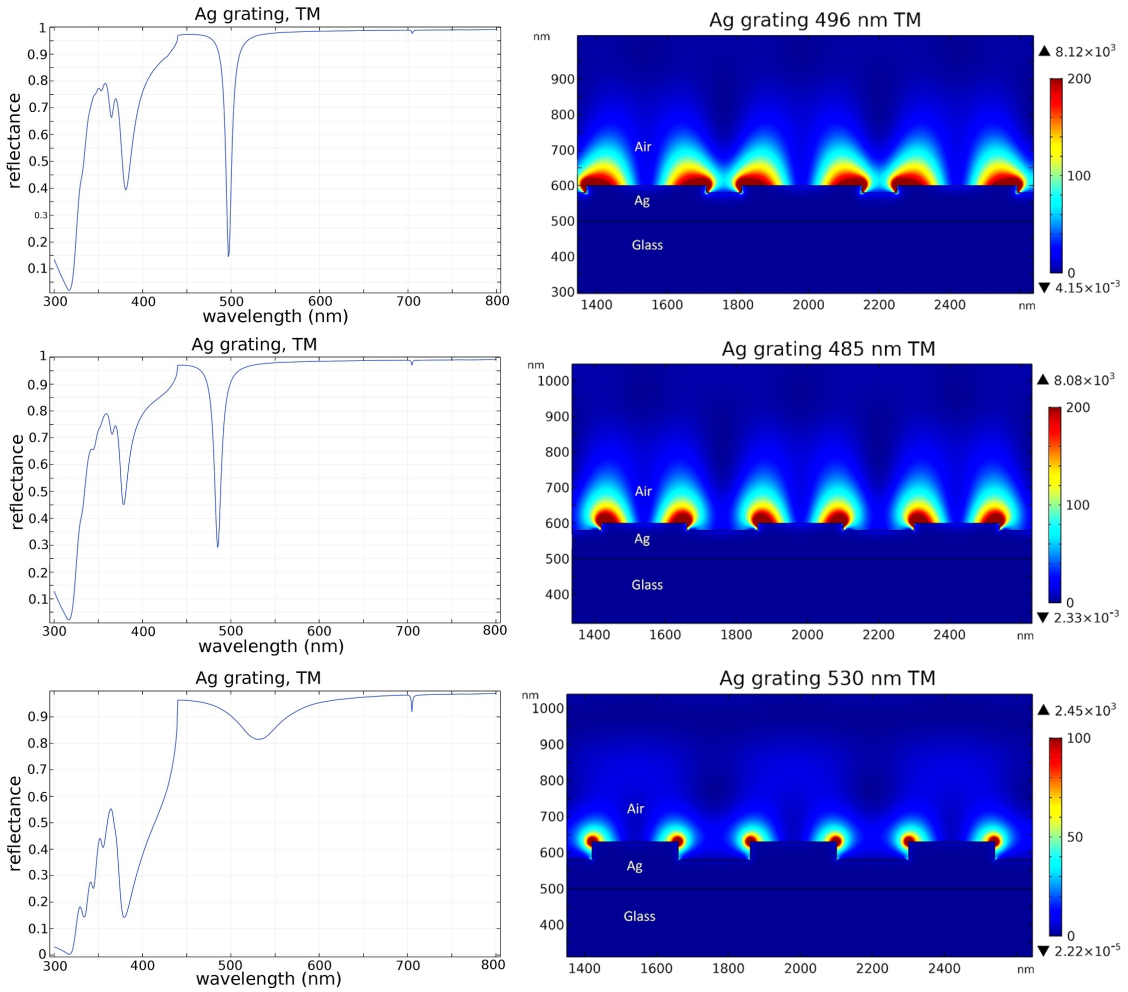

Figure 22: The reflectance spectra of three metal gratings with different parameters, and the electric field of each at resonance. The period of all gratings is 440 nm, and the thickness of the metal layer 80 nm. In the first grating the grating width is 340 nm, and the grating height 20 nm. In the second grating the width is reduced to 240 nm. In the third grating the height is also increased to 50 nm.

The spectra for all three gratings show a distinct edge at the wavelength corresponding to the grating period. The behaviour of the grating abruptly changes at this wavelength, with the grating starting to act as a reflective surface for wavelengths above it, except for the resonant wavelength. At lower wavelengths, the grating diffracts light, causing the large dips visible in the spectra. The smaller dips correspond with localized surface plasmons, which greatly enhance the electric field in a few nanometers radius around the sides of the gratings. Coupling to the more useful propagating surface plasmon occurs at wavelengths slightly above the grating period. The position and depth of the dip in the reflectance spectrum depends on the dimensions of the grating. Increasing the grating period also increases the resonant wavelength in proportion. Increasing the height and width of the grating structures moves the dip to a higher wavelength, further from the grating period. Increasing the height of the grating also makes the dip position depend more strongly on the width of the grating structures. Based on the simulations, there seems to be an optimal grating height, close to 20 nm, where all light is coupled to the surface plasmons. This produces a very sharp dip in the spectrum, indicating strong resonant behaviour.

One problem with silver gratings is oxidation of the silver. This can easily be fixed, by adding a thin dielectric layer on top of the grating to protect the silver. However, this dielectric layer adversely affects the electric field enhancement achieved by the grating, by trapping a part of the enhanced field in the dielectric layer. Figure 23 shows the above first silver grating covered by a 10 nm thick layer of Al_2O_3. In this case, the resonant wavelength increases to 536 nm. This is caused by the increased refractive index at the grating surface, making the grating period effectively larger. The electric field enhancement on top of the grating is also noticeably weaker than with the bare metal grating, and more confined to the corners.

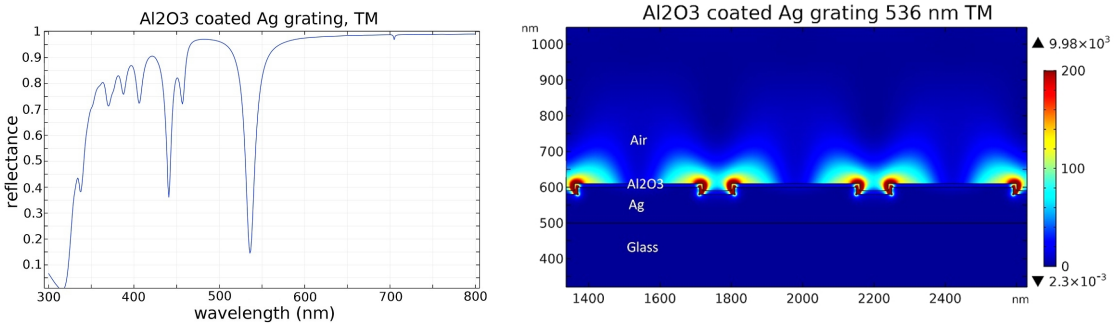

Figure 23: Reflectance spectrum and electric field of silver grating covered by 10 nm Al_2O_3. The grating period is 440 nm, the grating width 340 nm and the grating height 20 nm.

4.4 Metal gratings on cavities

Next, coupling between the cavity mode and surface plasmon is examined. In order to do this, the top metal layer of the cavity is patterned with a grating structure, with a resonant wavelength matching that of the cavity. This is expected to create an interaction between the surface plasmon and cavity mode, and may enable further enhancement of the electric field. A cavity consisting of a 80 nm thick layer of silver on the bottom, 106 nm thick layer of Al_2O_3 and a 50 nm thick silver layer on the top, with a 20 nm high metal grating with grating period 440 nm and grating width 340 nm, placed on the top layer, is simulated. Figure 24 shows the reflectance spectra and electric fields of both grating and cavity individually, and the combined structure, in both TM and TE polarizations. The cavity on its own is resonant at 497 nm and the grating at 498 nm. With the grating placed on top of the cavity, the total structure is resonant at 504 nm, indicating a very small increase in the resonant wavelength. The electric field of the combined structure is very close to that of the grating alone, although the enhancement on top of the grating is slightly lesser. There is also some electric field confined in the cavity below the gaps in the grating. This suggests that part of the incident wave couples to the grating and part to the cavity, making both weaker. Overall, there seems to be very little interaction between the two modes, suggesting a thinner metal layer might be needed between the grating and cavity. When irradiated with TE polarized light, the combined structure behaves as a cavity, with a resonant wavelength at 496 nm. The coupling to the cavity is also weakened, due to the added thickness from the grating.

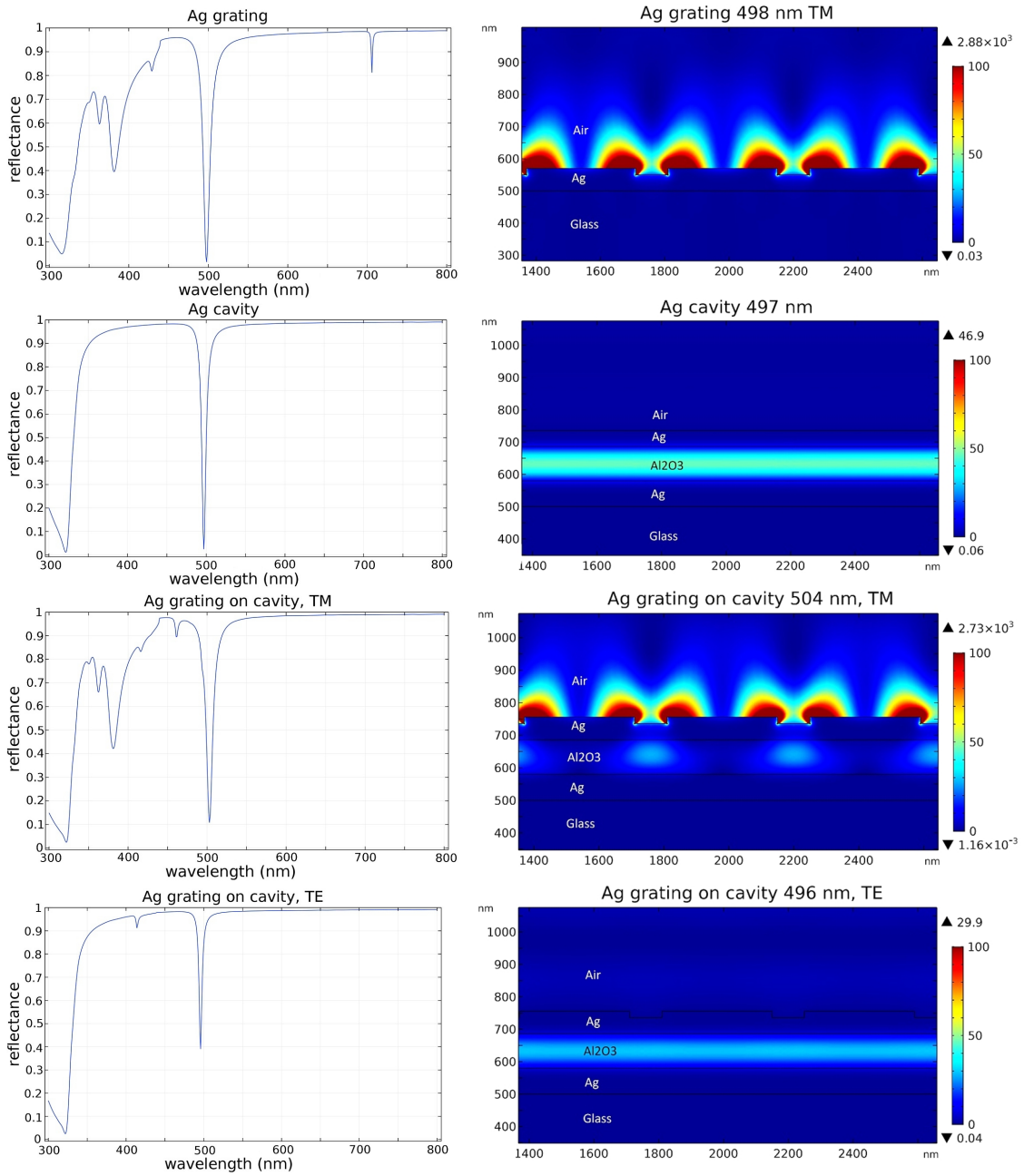

Figure 24: Reflectance and electric field distribution of metal grating, cavity and grating on cavity in TM and TE polarizations. The thick top layer of the cavity causes the interaction between the two modes to remain quite weak, with the grating clearly dominating the behaviour of the combined structure.

By decreasing the silver layer thickness under the grating to 30 nm, a clear separation appears between the two resonant dips caused by cavity and metal grating, as seen in figure 25. The resonant wavelength of the grating is pushed higher, while the resonant wavelength of the cavity remains roughly the same. This is somewhat contrary to the expected behaviour, where making the top layer thinner should shift the resonant wavelength of the cavity higher, suggesting that the two phenomena are interacting with each other, forcing the two resonant dips apart. However, this interaction does not seem to be very beneficial, as both dips are shallower than in the individual structures, and the electric fields are weaker.

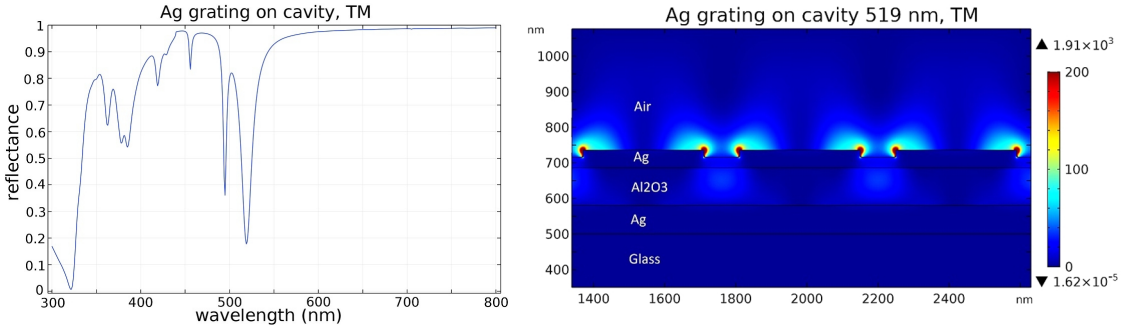

Figure 25: Metal grating on cavity with 30 nm top layer thickness in TM polarization. The two dips caused by grating and cavity are now distinguishable from each other, due to being forced apart by the interacting modes.

Reducing the periodicity of the grating to 400 nm causes both dips to move to a lower wavelength, while maintaining the separation between them, indicating that the separation in resonant wavelengths is indeed caused by coupling between the two effects. In this grating, another dip also appears at 441 nm, as shown in figure 26. At this wavelength, the electric field on top of the grating looks similar to the one at the resonant wavelength, while the field in the cavity has an additional maximum directly under the grating.

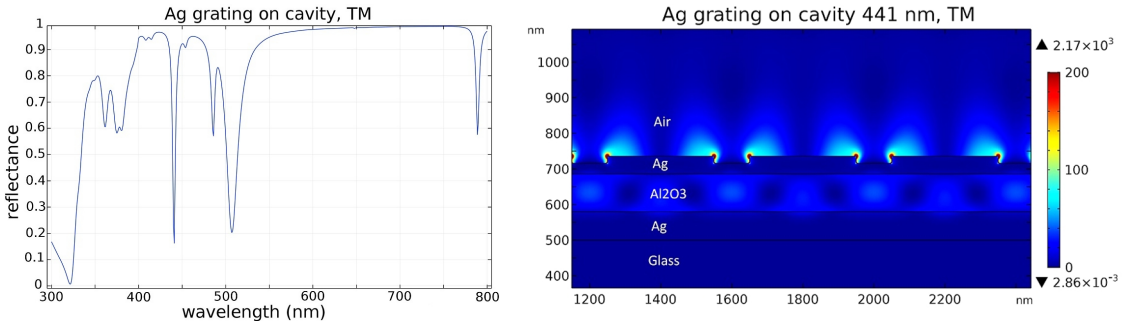

Figure 26: Metal grating on cavity with the grating period reduced to 400 nm. The separation between dips remains almost constant, despite the reduced period. There is also another dip appearing at 441 nm, suggesting a different type of interaction between the two phenomena.

This behaviour is examined further by increasing the Al_2O_3 thickness to 135 nm and the grating period to 460 nm. As shown in figure 27, this causes three distinct dips in the spectrum. The two higher wavelength dips correspond to the resonant wavelengths of the grating and cavity, which now occur at separate wavelengths. However, a third dip also appears at 497 nm, which appears to be caused by an interaction between the grating and cavity. This creates a strong electric field enhancement above the grating, which is almost equal to the enhancement of the grating on its own. Inside the cavity, the electric field has maxima located directly below both the spacing and the grating elements. The shape of the electric field suggests it may be caused by interference of diffracted waves. With TE polarized light, mainly the cavity resonance at 588 nm is observable, although there is a small resonant dip at 465 nm. At this wavelength the electric field seems to form a standing wave also in the x-direction in the cavity.

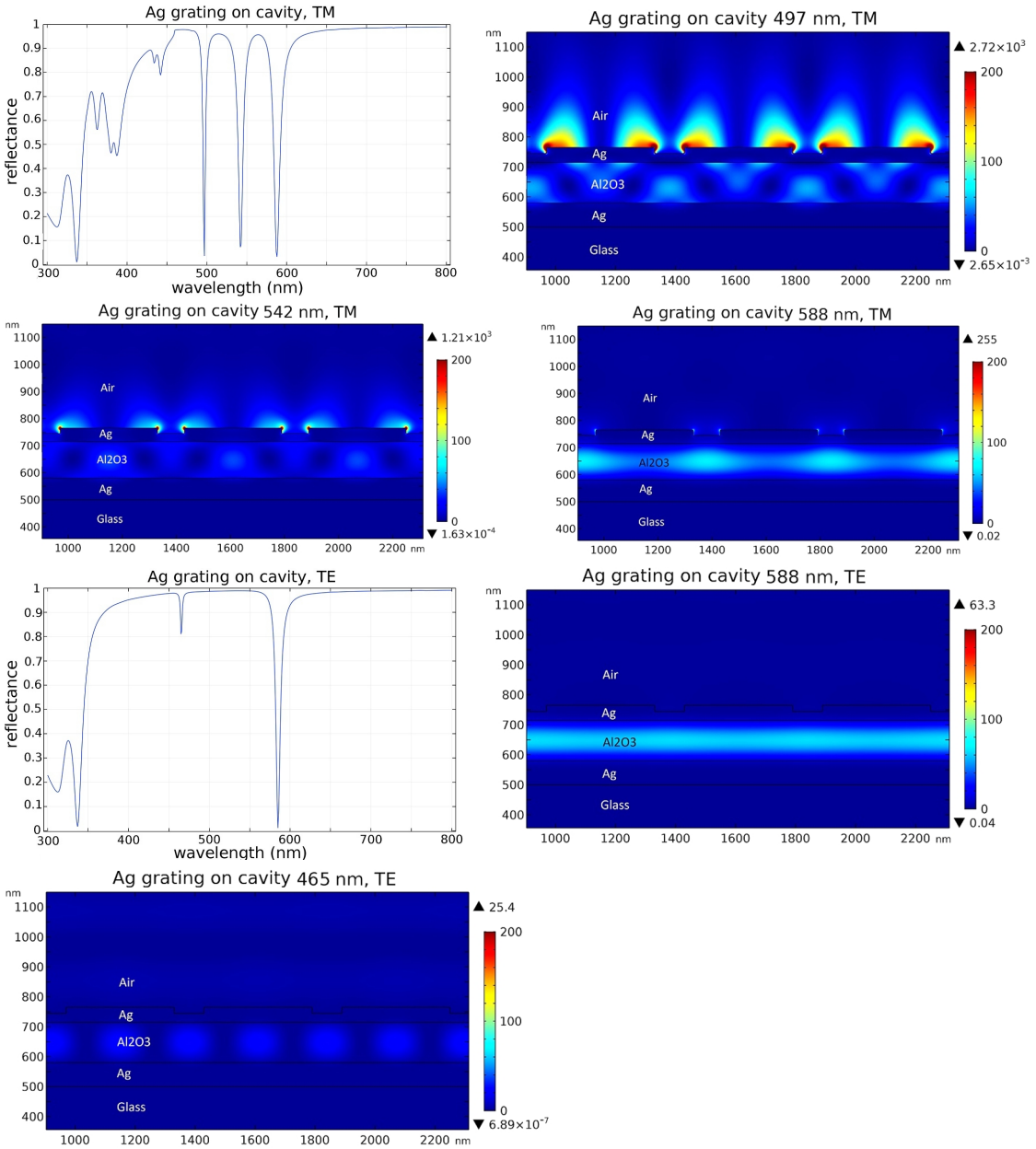

Figure 27: Simulated spectra and electric field intensities in TE and TM polarization of a silver grating with 460 nm period, 340 nm grating width and 20 nm grating height, on a cavity with 135 nm AL_2O_3. In TM, three major dips are visible at 497 nm, 542 nm and 588 nm. In TE the dip at 588 nm is visible, along with a small dip at 465 nm.

Another type of grating is also tested on top of the cavity, where the top metal layer is patterned with a grating fully etched through the metal. This type of grating can cause coupling between plasmon and cavity modes, altering the behaviour of both [31]. First, 20 nm thick grating strips with 450 nm grating period and 300 nm width are placed instead of the top layer on a cavity. The thickness of the Al_2O_3 layer is only 100 nm, to compensate the increase in resonant wavelength due to the effectively thinner top layer. The spectrum and electric fields of this structure simulated with TM polarized light are shown in figure 28. The resonant wavelengths of both cavity and grating coincide at 510 nm, creating one clear dip in the reflectance spectrum. At this wavelength, an

enhancement of the electric field of up to 100 can be observed both directly on top of and below the grating. This suggests a coupling between the plasmonic modes on the two interfaces of the metal, as well as with the cavity. A sharp dip can also be seen at 719 nm. This is caused by coupling to surface plasmons on the far side of the bottom metal layer, at the interface between metal and glass. Despite the 80 nm thick silver layer, a very high electric field enhancement can be observed, suggesting that this type of structure could also be useful for exciting surface plasmons in a transmission setup.

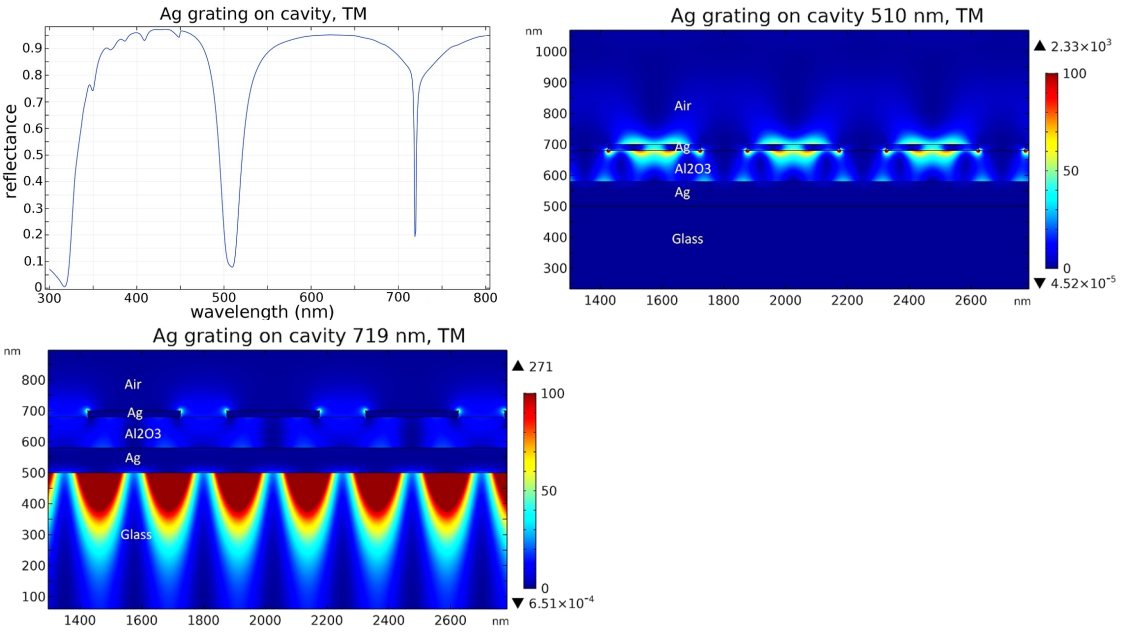

Figure 28: TM Reflectance spectrum and electric field at resonance of a metal grating consisting of 20 nm thick strips of silver placed as top layer of a cavity. The grating period is 450 nm and the width of the strips is 300 nm, while the thickness of the Al_2O_3 layer is 100 nm. Two clear resonances appear in the spectrum, with plasmons excited on the surfaces of the silver strips and on the underside of the bottom layer respectively.

Due to the thin top layer, the structure only has a weak resonant dip in the TE spectrum, shown in figure 29. This resonance occurs at 545 nm, 35 nm higher than the dip in TM. At the resonant wavelength, the electric field is enhanced mainly under the gaps in the grating. A small portion of the enhanced electric field extends through the gaps, and may provide some enhancement outside the cavity, but most of the electric field enhancement is still confined inside the cavity.

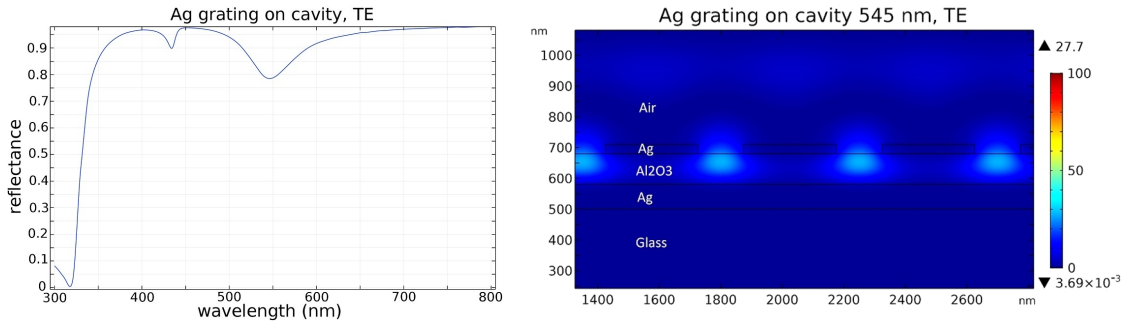

Figure 29: The above structure in TE polarization. A weak resonance is observable, caused by confinement in the cavity. This occurs at a higher wavelength than the resonance in TM polarization.

Increasing the metal grating thickness to 30 nm causes the two dips to separate to 485 nm and 495 nm, as shown in figure 30. At 485 nm the electric field is enhanced mainly inside the cavity, in a pattern of lines extending between the grating and the bottom metal layer. This pattern is likely formed by the diffraction caused by the grating interacting with the excited plasmons. At 495 nm, the electric field is strongly confined under the middle of the grating strips, with some electric field enhancement visible on top of the grating. The higher wavelength resonance seems to be caused by the cavity, as the enhancement is strongest under the gratings. Due to the thin top layer, and surface plasmons formed on top of it, the standing wave peak is not in the middle of the cavity, but closer to the top metal. Simulations show that the separation between the two dips depends on the grating spacing, with wider spacing pushing the dips further apart. With a spacing less than 50 nm, the two dips will coincide.

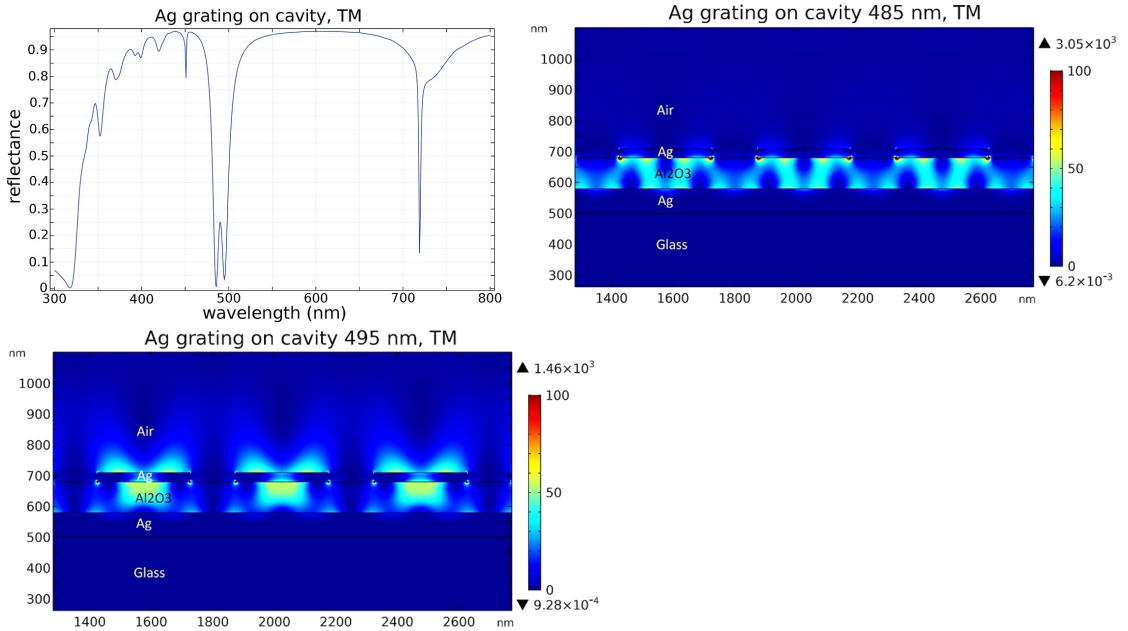

Figure 30: Metal grating with the thickness of silver strips increased to 30 nm, but other parameters kept the same. This causes two dips to separate around 490 nm.

Increasing the Al_2O_3 layer thickness to 120 nm causes the resonant wavelength of the cavity to increase. The simulated spectra and electric fields for both TM and TE

polarizations are shown in figure 31. In TM, the spectrum is now dominated by the resonance of the cavity, at 538 nm. At this wavelength, the electric field is strongly confined in the cavities formed under the silver strips, with a small enhancement on top of the strips, indicating some coupling to surface plasmons. In TE, the resonant wavelength of the cavity is at 610 nm, but there is also a strong dip at 465 nm. The electric field is again confined in the cavity under the silver strips, but there is an additional electric field maximum in the spacing between the strips. This may be caused by the grating acting as a DBR, causing confinement of the electric field along the x-axis. The cavity resonances for TE and TM polarized light occur at different wavelengths, likely due to the grating reflecting TE and TM polarized light differently.

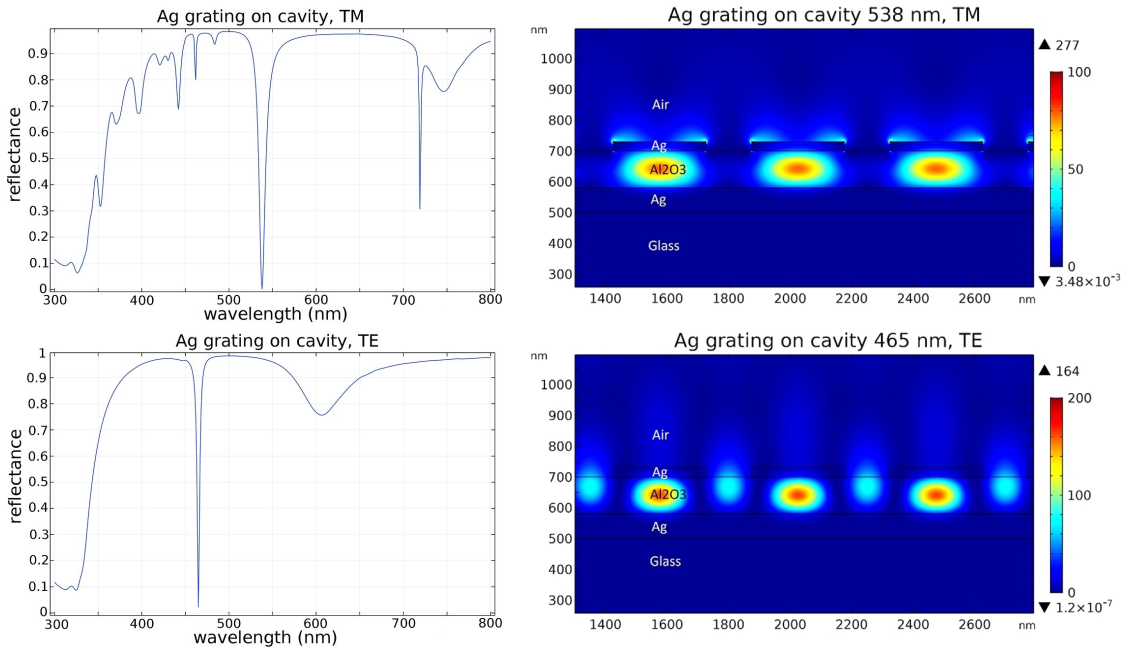

Figure 31: Metal grating with Al_2O_3 thickness increased to 120 nm. This creates one clear resonant dip in the reflectance spectra for both TE and TM polarizations.

By increasing the silver grating thickness to 40 nm, Al_2O_3 thickness to 140 nm and grating period to 460 nm, resonant wavelengths for both TE and TM polarization align at 495 nm, as shown in figure 32. In TE polarization the resonance is still caused by the cavities formed under the silver strips. In TM however, the cavity resonance seems to disappear completely. Instead, the electric field is now enhanced on top of the grating, indicating an efficient coupling to the surface plasmon on the grating. This plasmon seems to interact with the cavity creating an electric field enhancement similar to the silver grating alone. Having a resonant dip at the same wavelength for both polarizations creates the possibility of having a structure with very efficient coupling to the resonant modes when using unpolarised light.

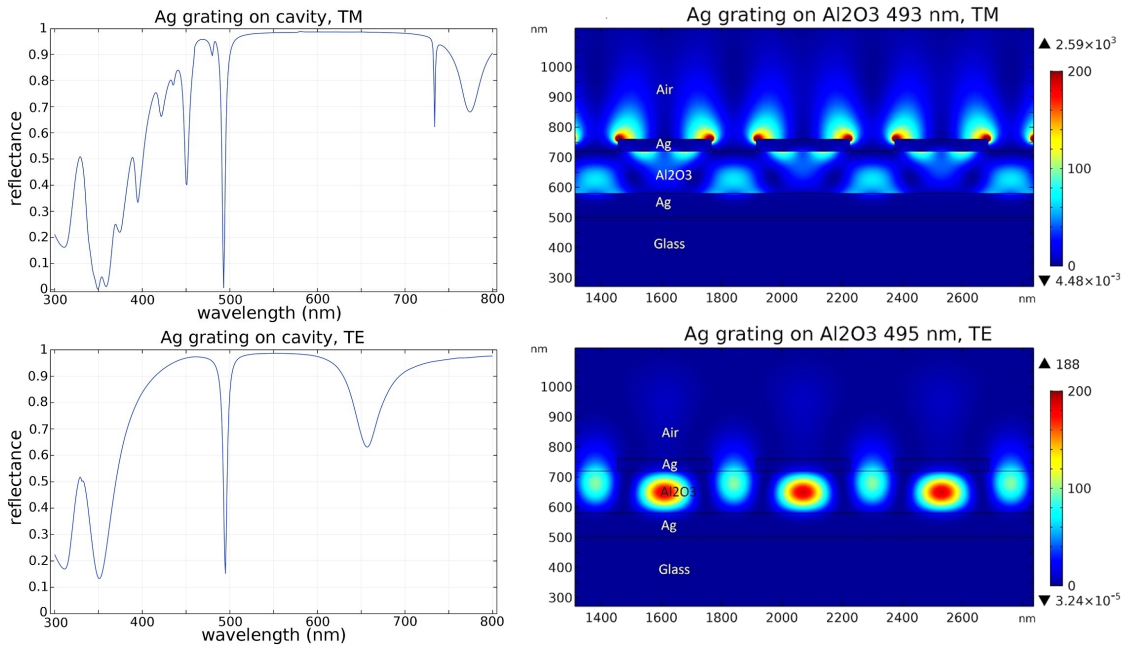

Figure 32: Metal grating with 40 nm thickness, 460 nm period and 300 nm width on a 140 nm Al_2O_3 layer. Both TM and TE polarizations now display a resonant dip at 495 nm. The TM mode provides high enhancement on top of the grating, while the TE mode is mostly confined in the cavity.

The simulations presented here have shown that the resonant effects of the metal grating and cavity can interact with each other, if appropriate structural parameters are used. In most cases, however, this seems to provide no clear benefit, as a large portion of the electric field is confined inside the cavity. With TM polarized light the electric field on top of the gratings can at best reach similar intensities as a grating alone. With TE polarized light, these structures could be more useful, as a grating alone simply acts as a reflective surface. A problem with TE modes shown here is that the electric field mostly is being confined in the cavity layer, with no obvious way to extract it, due to there being no surface plasmons to couple to. A possible solution to this could be using 3-dimensional structures, exciting surface plasmons in all directions.

4.5 Dielectric gratings

Instead of a metal grating, a dielectric grating on a plain metal surface can also be used to couple to surface plasmons [32]. In this case, the dielectric grating causes scattering, enabling coupling to surface plasmons. A 20 nm high Al_2O_3 grating is placed on top of an 80 nm thick silver surface. This causes a small dip in the reflectance spectrum at 493 nm, as shown in figure 33. An electric field enhancement of slightly more than 100 can be observed on the grating. This is weaker than the enhancement provided by a metal grating, but almost as strong as the enhancement from the metal grating covered by a 10 nm Al_2O_3 protective layer.

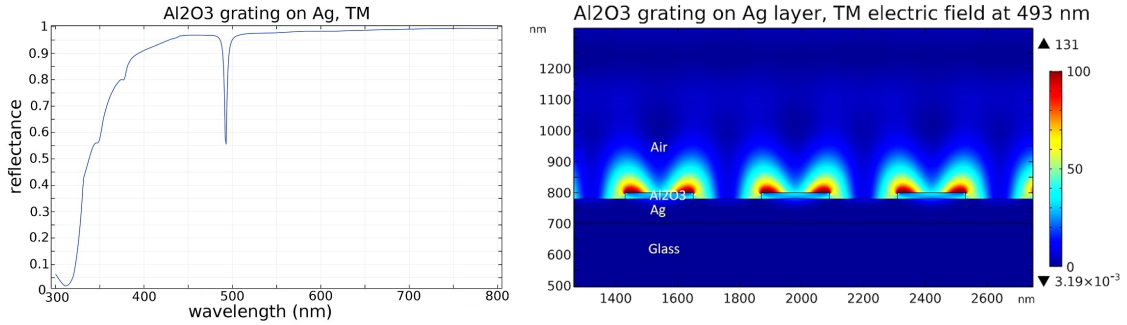

Figure 33: Al_2O_3 grating with 20 nm height, 440 nm period, and 220 nm width, on an 80 nm thick silver layer. The grating is able to provide coupling to the surface plasmons, although the effect is quite weak.

Adding a layer of Al_2O_3 under the grating makes the dip in the reflectance spectrum deeper and improves the electric field enhancement. By adding a 20 nm thick layer, the resonant wavelength is increased to 535 nm, as shown in figure 34, and the coupling is improved, as shown by the lowered reflectance. The electric field is further enhanced on top of the grating, now providing a stronger enhancement than the Al_2O_3 covered silver grating.

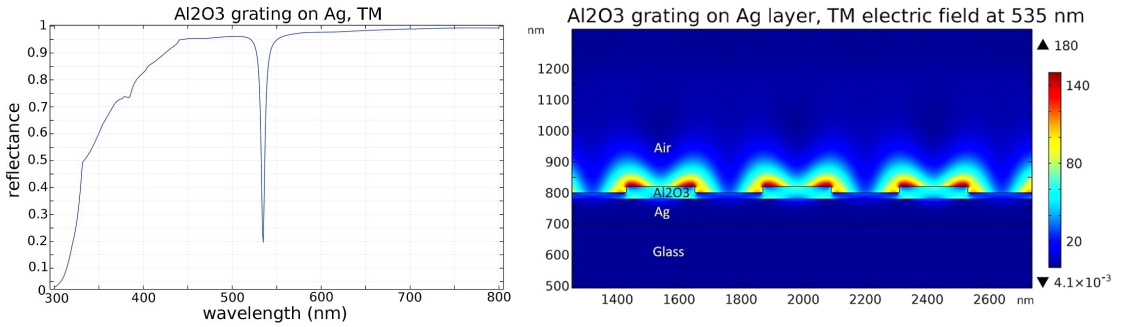

Figure 34: The same grating as in figure 33, but with a 20 nm Al_2O_3 layer added under it. This provides stronger coupling to the surface plasmon, while moving the resonant wavelength higher.

Unlike the metal grating, the dielectric grating also causes electric field enhancement using TE polarized light. By making the Al_2O_3 layer 80 nm thick, a sharp dip appears in the spectrum for TE polarized light at 488 nm, as shown in figure 35. This dip, however, appears at a different wavelength than the dip for TM polarized light, which is now at 677 nm. The dip in the TM spectrum is also very sharp. At this wavelength the electric field is enhanced on top of the metal surface, inside the Al_2O_3 layer, indicating that the incident light gets coupled to the surface plasmon mode.

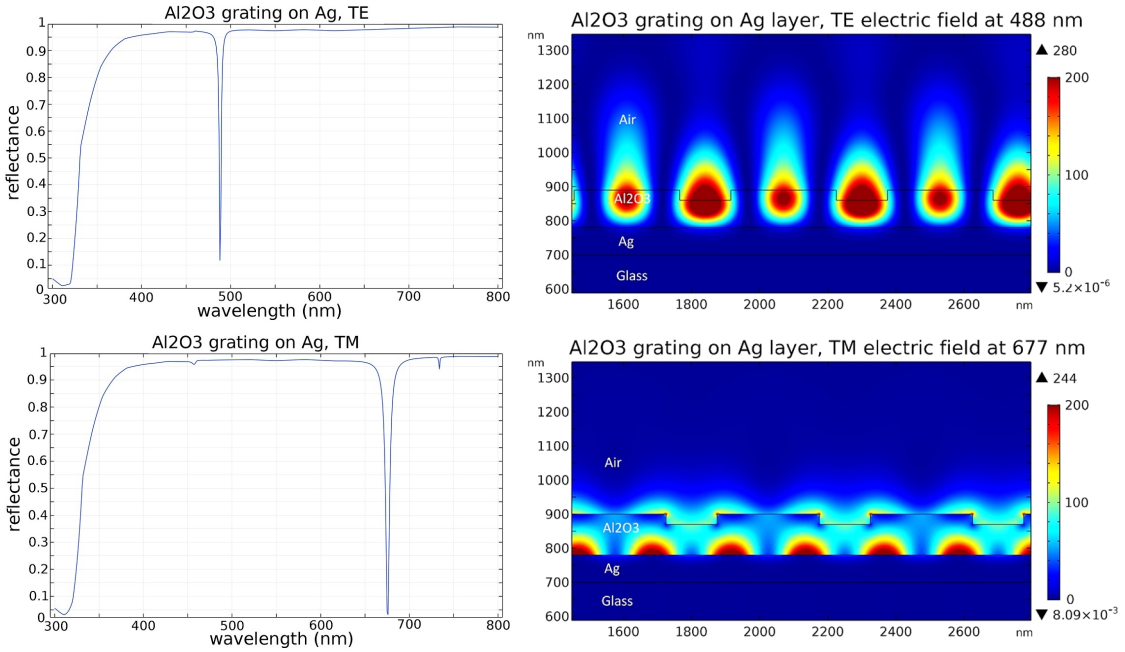

Figure 35: Al_2O_3 grating with an 80 nm layer under. This causes a dip to also appear in the TE spectrum, at 488 nm. With TM polarized light, the resonant wavelength is much higher, at 677 nm. Both polarizations show greatly enhanced electric fields, which are mostly confined in the dielectric layer.

Increasing the Al_2O_3 layer thickness further, to 200 nm, causes another dip to appear at a lower wavelength in the TM spectrum. At this wavelength the electric field is greatly enhanced on top of the Al_2O_3 grating instead of the boundary between silver and Al_2O_3.

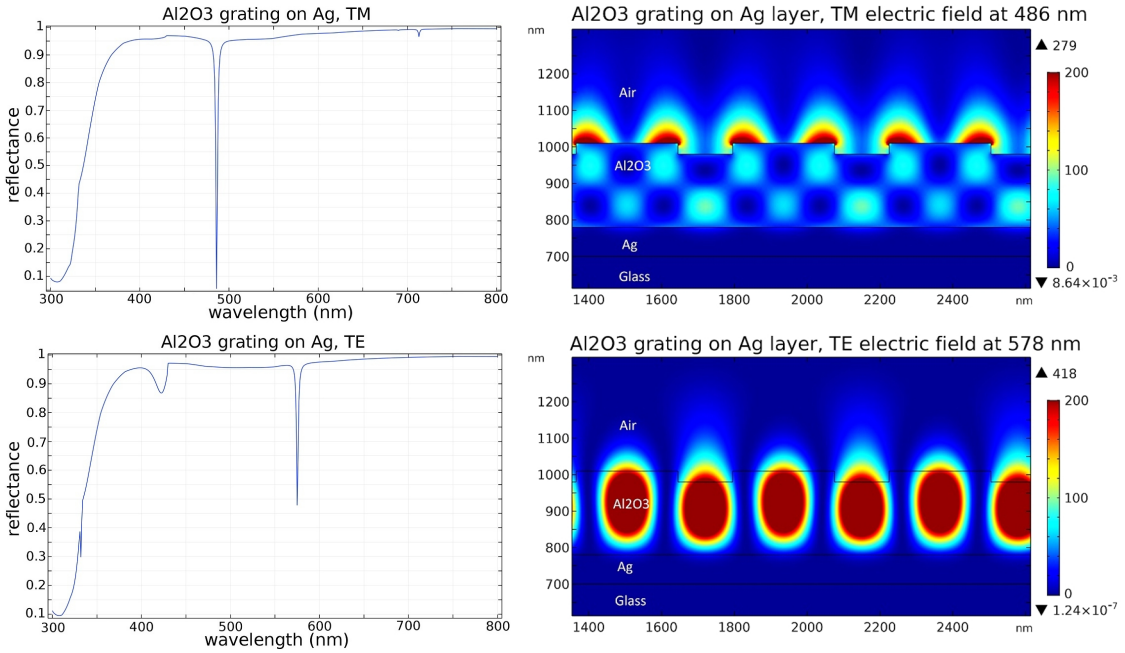

Figure 36: Increasing the Al_2O_3 thickness further to 200 nm causes another dip in the TM spectrum, where the electric field is mainly enhanced on top of the grating.

5 Conclusions

This thesis has investigated the enhancement of the electric near field, achievable by different resonant structures. The goal was to create a nanostructure with an intense electric field forming on top of it when irradiated with light of a certain wavelength. This structure could then be used as a substrate for spectroscopy and bioimaging applications.

First, the Tamm plasmon structure, consisting of a DBR with a metal layer on top, was investigated. This was done through simulations and measurements of a five layer DBR with a gold layer on top, followed by simulations of a nine layer DBR. The first five layer structures were unable to create sufficient confinement to cause a strong resonance, causing only a weak dip to be visible in the reflectance spectrum. The simulated nine layer structure performed better, allowing a clear resonant dip to form. Some modifications of the structure were tested, which suggest coupling to the resonant mode in the metal covered DBR can be improved by aligning the resonant wavelength of the combined structure with the reflectance peak of the DBR. Contrary to expectations, the electric fields formed in the Tamm plasmon structure showed no evidence of a surface wave. Instead, confinement of the electric field in a standing wave pattern, very similar to the mode formed in a cavity, could be seen at the resonant wavelength. This suggests that the metal covered DBR simply acts as a modified resonant cavity. One practical difficulty with this structure is that a very large number of dielectric layers is needed, in order to achieve efficient confinement.

Next, a simpler cavity design consisting of two metal layers with a dielectric layer between them, was investigated. This structure demonstrated the ability to either transmit or confine a very narrow range of wavelengths around the resonant wavelength, depending on the thicknesses of the metal layers. By adjusting the thicknesses of the metal layers properly, the cavity is able to almost fully absorb the incident light, causing a standing wave to form in the cavity, with an electric field intensity nearly 50 times that of the incident light.

Surface plasmons excited by grating coupling were also simulated, in order to find optimal parameters for the grating. For a resonant wavelength close to 500 nm, a 20 nm high silver grating with a period of 440 nm and a 340 nm width was found to offer the best coupling to the surface plasmons. In general, the resonant wavelength seems to be directly related to the grating period, and the grating seems to work best when the resonant wavelength is slightly above the period. This can be achieved by adjusting the grating height, with a higher grating being resonant further from the grating period. The width and spacing of the grating seem to have less impact on the performance of the grating ant the resonant wavelength, although this increases as the grating is made higher. In the gratings examined in this thesis, a width close to of ¾ of the grating period and a spacing close to ¼ was found to perform best.

The silver grating was then applied on the top layer of a cavity, in order to investigate the coupling between surface plasmon and cavity mode. Several different structural parameters were tested, displaying varying amounts of coupling between the two modes. In most cases however, this coupling appears to be detrimental to the enhancement, as part of the electric field is confined inside the cavity, weakening the enhancement on top of the structure. At best, electric field intensities comparable to the grating alone were achieved. Unlike the metal grating alone however, the combined structure also displayed resonant behaviour with TE polarized waves. This could make the structure useful for applications with unpolarised light, where both polarization directions play a role.

Lastly, dielectric gratings on top of a plain silver layer were simulated. These structures displayed resonant behaviour in both TM and TE polarizations, and provided promising electric field enhancement. One advantage of these structures compared to the silver gratings is that no separate capping layer needs to be added on top of the structure.

All of the structures examined in this thesis were able to provide substantial enhancements to the electric near field. This enhancement is in all cases achieved by coupling incident light into resonant modes, which are able to confine the light in the near field region. The confined light can then interfere constructively, forming strongly enhanced electric fields at certain locations in the structure.

The FEM simulation used in this thesis provided a useful tool for investigating the electric field inside and near the surface of the simulated structures. The reflectance spectra provided by the simulation was also able to accurately predict the reflectance behaviour of the measured samples. The only loss mechanisms limiting the enhancement in the simulations, were losses in the metal and through leakage radiation. Because of this, the actual electric field enhancements achievable may be slightly lower, as other loss mechanisms are present in reality. The simulation, when correctly set up, was able to quickly calculate the solutions, providing data that seems plausible. The simplicity of the equation used to solve electromagnetic fields minimizes the risk for errors, the complexity instead coming from the large number of points in which the field is solved. The acquired solutions can be assumed to satisfy Maxwell's equations under the given condition. The difficulty then is in interpreting weather the assumptions used in the simulations match the real world conditions closely enough to give results applicable in reality. For the multilayer structures this seems to be the case, but the grating structures will require testing before definite conclusions can be drawn.

References

[1] R. Gillibert, M. Sarkar, J.-F. Bryche, R. Yasukuni, J.Moreau, M. Besbes, G. Barbillon, B. Bartenlian, M.Canva and M. L. de la Chapelle, "Directional surface enhanced Raman scattering on gold nano-gratings", *Nanotechnology*, vol. 27, pp. 115202, 2016.

[2] J. Homola, S. S. Yee, G. Gauglitz, "Surface plasmon resonance sensors: review", *Sensors and actuators. B*, vol. 54, pp. 3, 1999.

[3] X. D. Hoaa, A. G. Kirk, M. Tabrizian, "Towards integrated and sensitive surface plasmon resonance biosensors: A review of recent progress", vol. 23, pp. 151, 2007.

[4] F. Ye, J.M. Merlo, M. J. Burns and M. J. Naughton, "Optical and electrical mappings of surface plasmon cavity modes", *Nanophotonics*, vol. 3, pp. 33, 2007.

[5] V. Ntziachristos, "Fluorescence Molecular Imaging", *Annual review of biomedical engineering*, vol. 8, pp. 1, 2006.

[6] E. Le Moal, E. Fort, S. Lévêque-Fort, F. P. Cordelières, M.-P. Fontaine-Aupart and C. Ricolleau, "Enhanced Fluorescence Cell Imaging with Metal-Coated Slides" *Biophysical Journal*, vol. 92, pp. 2150, 2007.

[7] F. Tam, G. P. Goodrich, B. R. Johnson and N.J. Halas, "Plasmonic Enhancement of Molecular Fluorescence", *Nano letters*, vol. 7, pp. 496, 2007.

[8] W. L. Barnes, A. Dereux and T. W. Ebbesen, "Surface plasmon subwavelength optics", *Nature*, vol. 424, pp. 824, 2003.

[9] E. Ozbay, "Plasmonics: Merging Photonics and Electronics at Nanoscale Dimensions", *Science*, vol. 311, pp. 189, 2006.

[10] V. Amendola, R. Pilot, M. Frasconi, O. M. Maragò, M. A. Iatì, "Surface plasmon resonance in gold nanoparticles: a review", *Journal of physics. Condensed matter*, vol. 29, pp. 203002, 2017.

[11] J. M. Pitarke, V. M. Silkin, E. V. Chulkov and P. M. Echenique, "Theory of surface plasmons and surface-plasmon polaritons", *Reports on progress in physics*, vol. 70, pp. 1, 2006.

[12] R. H. Ritchie, "Plasma losses by fast electrons in thin films", *Physical review*, vol. 106, pp. 874, 1957.

[13] S. A. Maier and H. A. Atwater, "Plasmonics: Localization and guiding of electromagnetic energy in metal/dielectric structures", *Journal of Applied Physics*, vol. 98, pp. 10, 2005.

[14] E. Kretschmann and H. Raether, “Radiative decay of nonradiative surface plasmons excited by light”, *Zeitschrift für Naturforschung. A*, vol. 23, pp. 2135, 1968.

[15] A. Otto, “Excitation of Nonradiative Surface Plasma Waves in Silver by the Method of Frustrated Total Reflection”, *Z. Physik*, vol. 216, pp. 398, 1968.

[16] Y. Y. Teng and E. A. Stern, “Plasma radiation from metal grating surfaces”, *Phys. Rev. Lett.*, vol. 19, pp. 511, 1967.

[17] J. M. Elson and R. H. Ritchie, “Photon Interactions at a Rough Metal Surface”, *Physical Review B*, vol. 4, pp. 4129, 1971.

[18] K. A. Willets and R. P. Van Duyne, “Localized surface plasmon resonance spectroscopy and sensing”, *Annual Review of Physical Chemistry*, vol. 58, pp. 267, 2007.

[19] R. H. Ritchie, E. T. Arakawa, J. J. Cowan and R. N. Hamm, “Surface-plasmon resonance effect in grating diffraction”, *Physical review letters*, vol. 21, pp. 1530, 1968.

[20] M. D. Arnold and M. G. Blaber, “Optical performance and metallic absorption in nanoplasmonic systems”, *Optics express*, vol. 17, pp. 3835, 2009.

[21] P. R. West, S. Ishii, G. V. Naik, N. K. Emani, V. M. Shalaev and A. Boltasseva, “Searching for better plasmonic materials”, *Laser & photonics reviews*, vol. 4, pp. 795, 2010.

[22] M. A. Kaliteevski, I. Iorsh, S. Brand, R. A. Abram, J.M. Chamberlain, A. V. Kavokin and I. A. Shelykh, “Tamm plasmon-polaritons: Possible electromagnetic states at the interface of a metal and a dielectric Bragg mirror”, *Physical review B*, vol. 76, pp. 165415, 2011.

[23] S. J. Orfanidis, *Electromagnetic Waves and Antennas*, Rutgers University, 2002.

[24] M. E. Sasin, R. P. Seisyan, M. A. Kalitteevski, S. Brand, R. A. Abram, J. M. Chamberlain, A. Yu. Egorov, A. P. Vasil’ev, V. S. Mikhrin, and A. V. Kavokin, “Tamm plasmon polaritons: Slow and spatially compact light”, *Applied physics letters*, vol. 92, pp. 251112, 2008.

[25] Y. Chen, D. Zhang, L. Zhu, Q. Fu, R. Wang, P. Wang, H. Ming, R. Badugu and J. R. Lakowicz, “Effect of metal film thickness on Tamm plasmon-coupled emission”, *Phys. Chem. Chem. Phys.*, vol. 16, pp. 25523, 2014.

[26] K. J. Vahala, “Optical microcavities”, *Nature*, vol. 424, no. 6950, pp. 839, 2003.

[27] H. Becker, S. E. Burns, N. Tessler, and R. H. Friend, “Role of optical properties of metallic mirrors in microcavity structures”, *Journal of Applied Physics*, vol. 81, pp. 2825, 1997.

[28] R. Ameling and H. Giessen, “Microcavity plasmonics: strong coupling of photonic cavities and plasmons”, *Laser & photonics reviews*, vol. 7, pp. 141, 2013.

[29] K.M. McPeak, S. V. Jayanti, S. J. P. Kress, S. Meyer, S. Iotti, A. Rossinelli, and D. J. Norris, "Plasmonic films can easily be better: Rules and recipes", *ACS Photonics*, vol. 2, pp. 326, 2015.

[30] "The Finite Element Method (FEM)", https://www.comsol.com/multiphysics/finite-element-method, Accessed: 11.1.2018

[31] P. Jouy, Y. Todorov, A. Vasanelli, R. Colombelli, I. Sagnes, and C. Sirtori, "Coupling of a surface plasmon with localized subwavelength microcavity modes", *Applied physics letters*, vol. 98, pp. 021105, 2011.

[32] S. Park, G. Lee, S. H. Song, C. H. Oh, and P. S. Kim, "Resonant coupling of surface plasmons to radiation modes by use of dielectric gratings", *Optics letters*, vol. 28, pp. 1870, 2003.